Modeling springtime shallow frontal clouds with cloud-resolving and single-column models

Kuan-Man Xu,[1] Minghua Zhang,[2] Zachary A. Eitzen,[1,3] Steven J. Ghan,[4] Stephen A. Klein,[5,6] Xiaoqing Wu,[7] Shaocheng Xie,[8] Mark Branson,[9] Anthony D. Del Genio,[10] Sam F. Iacobellis,[11] Marat Khairoutdinov,[9] Wuyin Lin,[2] Ülrike Löhmann,[12,13] David A. Randall,[9] Richard C. J. Somerville,[11] Yogesh C. Sud,[14] Gregory K. Walker,[14] Audrey Wolf,[10] J. John Yio,[8] and Junhua Zhang[12]

Received 22 June 2004; revised 8 October 2004; accepted 10 November 2004; published 21 April 2005.

[1] This modeling study compares the performance of eight single-column models (SCMs) and four cloud-resolving models (CRMs) in simulating shallow frontal cloud systems observed during a short period of the March 2000 Atmospheric Radiation Measurement (ARM) intensive operational period. Except for the passage of a cold front at the beginning of this period, frontal cloud systems are under the influence of an upper tropospheric ridge and are driven by a persistent frontogenesis over the Southern Great Plains and moisture transport from the northwestern part of the Gulf of Mexico. This study emphasizes quantitative comparisons among the model simulations and with the ARM data, focusing on a 27-hour period when only shallow frontal clouds were observed. All CRMs and SCMs simulate clouds in the observed shallow cloud layer. Most SCMs also produce clouds in the middle and upper troposphere, while none of the CRMs produce any clouds there. One possible cause for this is the decoupling between cloud condensate and cloud fraction in nearly all SCM parameterizations. Another possible cause is the weak upper tropospheric subsidence that has been averaged over both descending and ascending regions. Significantly different cloud amounts and cloud microphysical properties are found in the model simulations. All CRMs and most SCMs underestimate shallow clouds in the lowest 125 hPa near the surface, but most SCMs overestimate the cloud amount above this layer. These results are related to the detailed formulations of cloud microphysical processes and fractional cloud parameterizations in the SCMs, and possibly to the dynamical framework and two-dimensional configuration of the CRMs. Although two of the CRMs with anelastic dynamical frameworks simulate the shallow frontal clouds much better than the SCMs, the CRMs do not necessarily perform much better than the SCMs for the entire period when deep and shallow frontal clouds are present.

Citation: Xu, K.-M., et al. (2005), Modeling springtime shallow frontal clouds with cloud-resolving and single-column models, *J. Geophys. Res.*, *110*, D15S04, doi:10.1029/2004JD005153.

[1]Climate Science Branch, NASA Langley Research Center, Hampton, Virginia, USA.
[2]Institute for Terrestrial and Planetary Atmospheres, Marine Sciences Research Center, Stony Brook University, Stony Brook, New York, USA.
[3]Also at Science Applications International Corporation, Hampton, Virginia, USA.
[4]Atmospheric Sciences Division, Pacific Northwest National Laboratory, Richland, Washington, USA.
[5]NOAA Geophysical Fluid Dynamics Laboratory, Princeton University, Princeton, New Jersey, USA.
[6]Now at Lawrence Livermore National Laboratory, Livermore, California, USA.
[7]Department of Geological and Atmospheric Sciences, Iowa State University, Ames, Iowa, USA.
[8]Lawrence Livermore National Laboratory, Livermore, California, USA.
[9]Department of Atmospheric Science, Colorado State University, Fort Collins, Colorado, USA.
[10]NASA Goddard Institute for Space Studies, New York, NY, USA.
[11]Scripps Institution of Oceanography, University of California, San Diego, La Jolla, California, USA.
[12]Department of Physics and Atmospheric Sciences, Dalhousie University, Halifax, Nova Scotia, Canada.
[13]Now at Institute for Atmospheric and Climate Science, Eidgenossische Technische Hochschule, Zurich, Switzerland.
[14]Climate and Radiation Branch, NASA Goddard Space Flight Center, Greenbelt, Maryland, USA.

0148-0227/05/2004JD005153$09.00

1. Introduction

[2] The representation of clouds in global climate models (GCMs) has become more complicated than a decade ago. For example, nearly every GCM uses a prognostic cloud microphysics parameterization to represent stratiform clouds and convective anvils rather than treating them as a simple grid-scale condensation. This progress can be attributed to the pioneering work of *Sundqvist* [1978]. The prognostic cloud parameterization approach uses prognostic equations to predict grid-mean cloud condensate. The advantages of this approach are that cloud formative and dissipative processes are explicitly included, the latent heat effects and the radiative effects of clouds are physically linked and a consistent coupling of convective and stratiform parameterizations are achieved by treating the detrained condensate water from convective towers as a source for the formation of stratiform clouds. Refinements of this approach have focused upon improving the formulations of sources and sinks of cloud water/ice associated with phase changes and the treatments of detrainment from convective towers [*Smith*, 1990; *Del Genio et al.*, 1996; *Fowler et al.*, 1996; *Lohmann and Roecker*, 1996; *Rotstayn*, 1997; *Rotstayn et al.*, 2000; *Rasch and Kristjánsson*, 1998; *Sud and Walker*, 1999; *Zhang et al.*, 2003], as well as the formulations of subgrid cloud amount or fractional cloudiness [*Tiedtke*, 1993; *Xu and Randall*, 1996]. Recently, an increasing amount of attention has been paid to the subgrid-scale inhomogeneity of stratiform clouds by adopting a probability density function (PDF) based approach to predict the cloud fraction and the distribution of subgrid-scale condensate [*Bony and Emanuel*, 2001; *Tompkins*, 2002].

[3] Despite the rapid progress in developing cloud parameterizations in the past decade, adequate measurements of cloud property distributions such as the vertical profiles of cloud condensate have not been available for the GCM community to comprehensively evaluate and further develop improved cloud parameterizations. In outlining the strategy for the Global Energy and Water-Cycle Experiment (GEWEX) Cloud System Study (GCSS) Working Group 4 (WG 4), *Moncrieff et al.* [1997, p. 844] stated: "A comprehensive evaluation of state-of-the-art cloud-resolving models will require state-of-the-art observations." Here cloud-resolving models (CRMs) are models that explicitly resolve cloud-scale dynamical processes. This statement applies equally well to the evaluation of cloud parameterizations in GCMs. One can adopt the single-column model (SCM) approach for the evaluation and further development of improved cloud parameterizations [*Randall et al.*, 1996]. Here an SCM is a single-column version of a GCM. In particular, observations of cloud properties and their related variables should be available, in addition to large-scale thermodynamic variables and radiative fluxes from the surface and the top of the atmosphere. Some recent field experiments have provided increasingly comprehensive observations of cloud properties, particularly, the U.S. Department of Energy's Atmospheric Radiation Measurement (ARM) program [*Stokes and Schwartz*, 1994; *Ackerman and Stokes*, 2003].

[4] Model intercomparison studies have become a popular avenue for comparing model performance using similar model configurations under identically prescribed large-scale meteorological conditions. The ARM Cloud Parameterization and Modeling (CPM) WG has conducted two studies to compare the performance of SCMs and CRMs for simulating summertime continental cumulus convection. The CPM WG Case 4 study is built on the ARM/GCSS intercomparison experiences in the areas of deep cumulus convection in the tropics [*Redelsperger et al.*, 2000; *Bechtold et al.*, 2000] and midlatitudes [*Ghan et al.*, 2000; *Xie et al.*, 2002; *Xu et al.*, 2002], as well as midlatitude frontal systems [*Ryan et al.*, 2000], to specifically address the parameterization of stratiform clouds in GCMs using comprehensive data obtained from an ARM springtime intensive operational period (IOP). The science theme of this case study is: what determines the cloud distributions in observations and in models? The outcome of this intercomparison exercise will help SCM and CRM modelers to evaluate the adequacy of current cloud microphysics parameterizations and hopefully improve the representation of physical processes that determine cloud distributions in climate models. The results of this intercomparison exercise are presented in two papers, with emphases on different types of frontal cloud systems. *Xie et al.* [2005] is devoted to the evaluation of cloud parameterizations for deep frontal clouds. The present paper is devoted to the evaluation of the simulations of persistent shallow frontal clouds, in particular, to understand the physical causes of inadequate simulations of shallow frontal clouds and the deficiencies in key elements of cloud parameterizations that cause the intermodel differences.

[5] An IOP occurring in March 2000 was dedicated to measure cloud property profiles by the ARM program. This period is also known as the cloud IOP. This IOP delivers the best measurements of cloud property profiles during the 14 years of the ARM program, although there are some limitations in using them to evaluate cloud parameterizations, as discussed below. During the cloud IOP, several fast-moving frontal cloud systems propagated through the ARM Clouds and Radiation Testbed (CART) domain. Cloud systems associated with large frontal systems were advected into and out of the CART domain. Owing to this advection, the magnitude and temporal behavior of cloud property profiles obtained from point measurements at the ARM Southern Great Plains (SGP) central facility may not correspond to the domain-averaged values of these profiles. For example, before a front passes the central facility, no clouds are observed by the instruments located at the central facility even though the CART domain is partially filled with the frontal clouds. This is a serious problem for temporal averages over a short period during the initial passage and the exiting stage of the frontal cloud systems. Therefore a strategy for alleviating this problem is to use longer-period averages.

[6] In addition, the advective forcing data that are used to drive all model simulations are representative of the CART domain average rather than a single point. This averages out any spatial structures representing unresolved dynamics from the forcing data [*Zhang and Lin*, 1997; *Zhang et al.*, 2001]. The simulated results are presumably representative of the CART domain averages, too. However, the forcing data even in a domain-averaged sense are incomplete because they lack information on the advection of hydro-

Table 1. Single-Column and Cloud-Resolving Models Participating in This Intercomparison Study[a]

Model Acronym	Full Model Name	Investigator(s)	Microphysics References
CSU SCM	Colorado State University	Branson and Randall	*Fowler et al.* [1996]
ECHAM5	ECMWF-Hamburg Version 5	J. Zhang and Lohmann	*Lohmann et al.* [1999]
GFDL	NOAA Geophysical Fluid Dynamics Laboratory AM2/LM2	Klein	*Rotstayn* [1997]; *Rotstayn et al.* [2000]; *Tiedtke* [1993]
GISS	NASA Goddard Institute for Space Studies	Del Genio and Wolf	*Del Genio et al.* [1996]
McRAS	Microphysics and Relaxed Arakawa-Schubert	Sud and Walker	*Sud and Walker* [1999]
PNNL	Pacific Northwest National Laboratory Version of NCAR CCM2 (Community Climate Model Version 2)	Ghan	*Ovtchinnikov and Ghan* [2005]; *Ghan et al.* [1997]; *Cotton et al.* [1986]
SCAM	Single-column version of NCAR Community Atmospheric Model	Lin and M. Zhang	*Rasch and Kristjánsson* [1998]; *Zhang et al.* [2003]
Scripps	Scripps Institution of Oceanography	Iacobellis and Somerville	*Iacobellis et al.* [2003]; *Tiedtke* [1993]
CSU SAM	Colorado State University System of Atmospheric Model	Khairoutdinov	*Khairoutdinov and Randall* [2003]; *Lin et al.* [1983]; *Rutledge and Hobbs* [1984]
ISU	Iowa State University CRM	Wu	*Clark et al.* [1994]; *Kessler* [1969]; *Koenig and Murray* [1976]
UCLA/LaRC	University of California-Los Angeles CRM at Langley Research Center	Xu	*Krueger et al.* [1995]; *Lin et al.* [1983]
ARPS/LaRC	Advanced Regional Prediction System at Langley Research Center	Eitzen	*Xue et al.* [2001]; *Lin et al.* [1983]; *Krueger et al.* [1995]

[a]References describing the original and modified cloud microphysics parameterizations in each model are listed. A more complete description of each model can be found in the work of *Xie et al.* [2005].

meteors into and out of the CART domain. Thus the simulated cloud systems are those locally generated via the imposed large-scale advective cooling and moistening tendencies, and do not include those generated by the horizontal advection of hydrometeors. Compared to the domain-averaged measurements of cloud properties, the simulations with these incomplete forcings would have a phase delay of a few hours and a reduced/enhanced amplitude of hydrometeor contents when there are cloud systems that are advected into/out of the domain. Another limitation is in the 2-D configuration of CRMs for simulating frontal cloud systems by imposing horizontally homogeneous forcings, especially for simulating narrow rain bands associated with frontogenesis [*Bénard et al.*, 1992] when the large-scale gradient (perpendicular to the 2-D CRM domain) of temperature is not imposed. This may be a serious issue for simulating the deep frontal cloud systems, but less so for simulating the shallow frontal cloud systems.

[7] It is obvious that the simulation of midlatitude frontal clouds with SCMs and CRMs is a difficult task because of the large gradients of thermodynamic and dynamical fields associated with fronts. *Ryan et al.* [2000] identified problems in applying SCMs to rapidly advecting baroclinic systems from their intercomparison study of an Australian cyclone system. The forcing imposed to the SCM simulations was derived from a high-resolution three-dimensional CRM simulation. Advective tendencies of hydrometeors were ignored. This might have contributed to the conclusion drawn by *Ryan et al.* [2000] that SCMs have problems in simulating frontal systems, but *Klein and Jakob* [1999] found that a composite of simulated frontal cloud systems is more sensitive to the assumptions applied to ice-phase microphysics than to the inclusion of hydrometeor advection. *Petch and Dudhia* [1998] performed a pair of simulations with and without the advective tendencies of hydrometeors for a summertime midlatitude situation. As in the work of *Ryan et al.* [2000], all forcing information used in the work of *Petch and Dudhia* [1998] was derived from a mesoscale model simulation. They concluded that it is important to simulate the correct timing of convective events by including the hydrometer advection. The present study differs from these earlier studies in that advective forcings are observationally derived and independent of model physics and that the simulated cloud properties are compared with those from cloud radar observations.

[8] In the following, a brief description of the models and their parameterizations is given in section 2. Section 3 presents the observational data and analysis used for this study. Intercomparison results are discussed in section 4. A summary of this study is provided in section 5.

2. Model Description and Design of Simulation

[9] This section gives a brief description of the models that participated in this intercomparison study, with a focus on these aspects of the models that are related to cloud parameterizations (SCMs) and cloud microphysical processes (both CRMs and SCMs). Table 1 provides the acronyms of the models and their full names, as well as the names of the participating scientists. Details of the various types of parameterizations used in SCMs and CRMs such as those of cumulus convection and radiative transfer can be found in the work of *Xie et al.* [2005]. The warm-phase cloud microphysics parameterizations used in both CRMs and SCMs and the major cloud formative and dissipative processes included in SCMs are emphasized below.

[10] A fundamental distinction between CRMs and SCMs lies in the spatial and temporal scales in which cloud microphysical processes are treated. In CRMs, dynamical processes are explicitly resolved and cloud microphysical processes operate on relatively fine spatial and temporal scales, while all cloud processes are parameterized in

SCMs. Many intuitive and physically comprehensive assumptions and tunable parameters have to be introduced in the cloud parameterization schemes used in all SCMs or GCMs, although the mathematical formulas for some of the cloud microphysical processes, as described below, are largely similar to those used in CRMs.

2.1. Cloud Microphysics Parameterizations Used in CRMs

[11] The cloud microphysics parameterizations that are used in many state-of-the-art CRMs are bulk formulations [see *Xu et al.*, 2002]. This approach classifies hydrometeors into several major categories (or classes) according to the microphysical characteristics of the hydrometeors and predicts several moments of the drop size distribution (DSD) rather than the DSD itself. Conversions among different hydrometeor categories such as autoconversion between cloud water and rainwater have to be formulated. Many of these conversion rates depend not only upon the mixing ratios of the hydrometeor species, but also depend highly upon the ambient temperature [*Lin et al.*, 1983; *Rutledge and Hobbs*, 1984]. One-moment bulk schemes only predict the bulk mass mixing ratios, while two-moment bulk schemes predict both the bulk mass mixing ratios and the number concentrations of hydrometeor categories (liquid, ice, snow, graupel/hail and rain).

[12] Four CRMs participated in this study, CSU SAM, ISU, UCLA/LaRC and ARPS/LaRC. The UCLA/LaRC and ARPS/LaRC CRMs use a modified *Lin et al.* [1983] scheme [*Krueger et al.*, 1995], while the microphysics in the CSU SAM is based upon a combination of *Lin et al.* [1983] and *Rutledge and Hobbs* [1984]. The CSU SAM predicts two water species, total water, which is a sum of water vapor and cloud condensate, and precipitating water. The cloud condensate mixing ratio is diagnosed by a simple "all-or-nothing" moist-adjustment scheme. The partitioning of different categories of cloud condensate and precipitating water depends upon the ambient temperature. The ISU CRM's microphysics parameterizations are based upon the *Kessler* [1969] scheme for warm phase and the *Koenig and Murray* [1976] scheme for ice phase. The latter predicts the mixing ratios and the number concentrations of slow and fast falling ice particles.

[13] Typical cloud microphysical processes that are included in CRMs are as follows. Water vapor increases due to the evaporation of rainwater and decreases by its deposition onto snow and graupel. Cloud water decreases through autoconversion to rain, accretion by rain, snow or graupel, conversion to snow by riming and deposition via Bergeron processes (the growth of cloud ice at the expense of cloud water). Rain water decreases through evaporation and increases below the melting level through melting of graupel and snow, autoconversion of cloud water and various accretion processes. In addition, saturation adjustment is invoked to remove extra water vapor over saturation in a cloudy grid and to evaporate cloud water in an unsaturated grid. This adjustment process is a large contributor to latent heat release. Other processes related to ice-phase clouds are not described here, for the sake of brevity.

[14] Despite the aforementioned similarities, detailed formulations of some processes can be different among the CRMs, such as the autoconversion from cloud water to rainwater. The simplest *Kessler* [1969] formula is used in the CSU SAM, which is conveniently expressed as

$$P_{raut} = \max[0, \alpha(q_c - q_{c_0})], \tag{1}$$

where α is the autoconversion rate coefficient and q_{c_0} is chosen to be 1.0 g kg^{-1}. More complicated formulas include a nonlinear dependency on q_c. Different q_{c_0} values are also used in different models to delay or accelerate the autoconversion process (Table 2; Figure 1). Both the UCLA/LaRC and ARPS/LaRC CRMs use the *Lin et al.* [1983] formulation, but with different thresholds. The ISU CRM uses the *Berry* [1968] formulation as modified by *Simpson and Wiggert* [1969], which also depends upon the prescribed number concentration of cloud water N_c.

2.2. Cloud Parameterizations Used in SCMs

[15] There are a few types of cloud parameterizations used in SCMs. One type is similar to the bulk formulations used in CRMs except for the simplification of some processes. The CSU SCM uses the bulk parameterization of *Rutledge and Hobbs* [1984] while the PNNL SCM adopts the microphysical parameterization from a cloud model [*Cotton et al.*, 1986; *Ghan et al.*, 1997]. Because fractional cloud amount is not diagnosed/predicted in the CSU SCM, threshold values used in the microphysical processes have to be reduced (Table 2). The rainwater and snow mixing ratios are diagnosed in the PNNL SCM. The PNNL SCM has adopted the *Smith* [1990] approach to diagnose cloud fraction from the assumed triangular PDF of total water.

[16] Another type of cloud parameterizations is based upon the classical *Sundqvist* [1978] approach. Two subregions of a grid box, either clear or cloudy, are considered. The cloudy region has a relative humidity (RH) of 100%. The GISS, SCAM and McRAS SCMs predict cloud condensate with one prognostic equation. Separate equations for cloud water and cloud ice mixing ratios are used in the ECHAM5 [*Lohmann and Roecker*, 1996] and GFDL SCMs [*Rotstayn*, 1997; *Rotstayn et al.*, 2000]. The Scripps SCM adopts the *Tiedtke* [1993] scheme. When only one prognostic equation is used, the phase of cloud condensate is determined by the ambient temperature. When two prognostic equations are used, microphysical processes of the mixed-phase clouds are sensitive to the liquid-ice transition temperatures used in the SCMs (Table 2).

[17] Parameterizations of cloud fraction use the diagnostic approach with either assumed PDFs or with RHs as predictors in McRAS, PNNL and SCAM SCMs. The GISS SCM predicts the cloud "volume" fraction with a threshold RH of 80%. The areal fraction is then determined from the volume fraction and the layer's stability [*Del Genio et al.*, 2005]. The assumed PDF approach can result in a simple relationship between cloud fraction and RH [*Smith*, 1990]. The RH approach also requires a minimum threshold RH for cloud formation. The most sophisticated fractional cloud parameterization is the one used in the ECHAM5 SCM [*Tompkins*, 2002], which predicts the PDF of total water mixing ratio. The cloud fraction is prognostically obtained in the Scripps and GFDL SCMs with the *Tiedtke* [1993] scheme.

Table 2. Details of Cloud Fraction Parameterization and Formulations of Selected Cloud Microphysics Processes Used in SCMs and CRMs

Model	Condensation/Evaporation	Autoconversion Formulation and Thresholds	Liquid-Ice Transition Temperature	Cloud Fraction
CSU	relaxed to saturation mixing ratio with a very short relaxation time	*Kessler* [1969]; 0.25 g kg^{-1}	(−20, 0) °C	$f = 1$ if $q_c + q_i + q_s > 10^{-2}$ g kg^{-1}; $f = 0$ otherwise
ECHAM5	determined from the prognostic β -PDF [*Tompkins*, 2002] scheme	function of qc and Nc [*Beheng*, 1994]; Nc is prescribed to be 220 cm^{-3} near the surface and decrease to 50 cm^{-3} at 100 hPa	(−35, 0) °C	prognostic β -PDF [*Tompkins*, 2002] scheme
GFDL	triangular PDF of total water to diagnose condensate [*Smith*, 1990; *Rotstayn*, 1997]	*Manton and Cotton* [1977]; 10.6 μm	(−40, 0) °C	prognostic *Tiedtke* [1993] scheme
GISS	difference between the convergence of available latent heat and the increase of RH	exponential function of cloud water content; 0.5 g m^{-3}	(−40, −10) °C	using RH diagnose grid-volume fraction, cloud fraction is determined from it based upon stability
McRAS	a combination of several processes; e.g., change of cloud fraction	exponential function of cloud water content; 0.3 g m^{-3}	N/A[a]	$f = 1 - [(1 - RH)/(1 - RH0)]1/2$
PNNL	triangular PDF of total water to diagnose condensate [*Smith*, 1990]	integrating over the triangular PDF of total water [*Ovtchinnikov and Ghan*, 2005]	N/A	triangular PDF of total water mixing ratio [*Smith*, 1990]
SCAM	changes of cloud fraction and clear-area RH and rainwater evaporation	*Manton and Cotton* [1977]; 5 μm; reduced coefficient by a factor of 10	(−20, 0) °C	$f = \max(\text{fRH}, f_c, f_{st}, f_{min})$, fi is from condensation (RH), convective detrainment (c), and boundary layer (st)
Scripps	changes of saturation mixing ratio and cloud fraction (cloud fraction does not change during evaporation)	exponential function of cloud water content; 0.3 g kg^{-1}	N/A	prognostic *Tiedtke* [1993] scheme
CSU SAM	"all-or-nothing" moist adjustment	*Kessler* [1969]; 1 g kg^{-1}	(−40, 0) °C	diagnosed from CRM grids where $q_c + q_i > 0.01q^*$
ISU CRM	instantaneous saturation adjustment	*Berry* [1968]	(−40, 0) °C	diagnosed from CRM grids where $q_c + q_i + q_s > 0.01q^*$
UCLA/LaRC	instantaneous saturation adjustment	*Lin et al.* [1983]; 0.5 g kg^{-1}	(−40, 0) °C	diagnosed from CRM grids where $q_c + q_i > 0.01q^*$
ARPS/LaRC	instantaneous saturation adjustment	*Lin et al.* [1983]; 2.0 g kg^{-1}	(−40, 0) °C	diagnosed from CRM grids where $q_c + q_i > 0.01q^*$

[a]N/A, not applicable.

[18] In prognostic cloud parameterization schemes, terms representing the formation of clouds and cloud water/ice due to convection, boundary layer turbulence, and stratiform condensation processes are included. Cloud water/ice is removed through evaporation and conversion of cloud droplets and ice to precipitation. Precipitation processes take into account the conversion of cloud water to precipitation from precipitation falling through a cloud, the Bergeron-Findeisen processes, and precipitation formation within ice clouds, etc. Different formulations of the condensation/evaporation processes and the autoconversion process in all SCMs are also listed in Table 2.

[19] The autoconversion formulation used in the GFDL and SCAM SCMs adopts the *Manton and Cotton* [1977] scheme. In this scheme, the autoconversion rate is proportional to $q_c^{7/3}$, with a threshold value q_{c_0} that depends upon the prescribed N_c. The *Beheng* [1994] formulation is used in the ECHAM5 SCM, which is proportional to $q_c^{4.7}$ and does not have a threshold value for activation of autoconversion. The PNNL SCM adopts the *Khairoutdinov and Kogan* [2000] formulation, which is proportional to $q_c^{2.47}$ and $N_c^{-1.79}$, but integrates over a triangular PDF [*Ovtchinnikov and Ghan*, 2005]. The GISS, McRAS and Scripps SCMs use the *Sundqvist et al.* [1989] formulation, which is expressed as

$$P_{raut} = C_0(q_c/f)\left\{1 - \exp\left[-\left(\frac{q_c}{fq_{c_0}}\right)^p\right]\right\}, \quad (2)$$

where C_0 is the limiting autoconversion rate, and p is a free parameter that determines the sensitivity of autoconversion rate; $p = 4$ in the GISS SCM, but $p = 2$ in the McRAS and Scripps SCMs. The threshold value is set to be 0.5 g kg^{-1} in the GISS SCM, 0.3 g kg^{-1} in the McRAS and Scripps SCMs, respectively. The values of C_0 are different between the McRAS and Scripps SCMs. The differences in the autoconversion rates can be clearly seen in Figure 1. It should be noted, however, that other microphysical processes can offset the autoconversion process so that the solution of a particular SCM/CRM may be far less sensitive than that expressed in Figure 1.

2.3. Design of Simulation

[20] One simulation is performed by each participating SCM and CRM group for this study. The observed large-

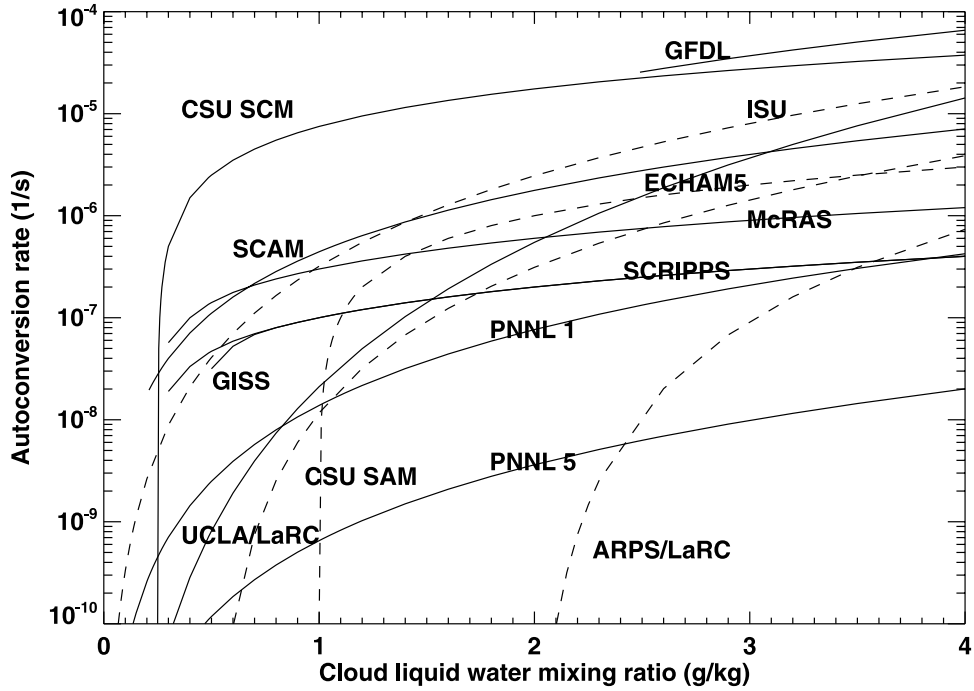

Figure 1. Autoconversion rates for CRMs (dashed lines) and SCMs (solid lines). Air density of 1 kg m^{-3} is used in the calculation of the autoconversion rates in all models except for the CSU SCM, CSU SAM and PNNL SCM whose autoconversion rates do not depend upon the air density. PNNL 1 uses the number concentration of 100 cm^{-3} while PNNL 5 uses the number concentration of 500 cm^{-3}. Details of the formulations of the autoconversion rates are discussed in the text and in Table 2.

scale advective cooling and moistening tendencies (see section 3) are imposed uniformly on model grid points in the horizontal domain and continuously in time. The observed diurnally varying surface sensible and latent heat fluxes are also imposed so that the land-surface processes are not interactive in all models. Interactive radiative transfer is used in all models. The domain size of the CRMs is about 500 km. The vertical/horizontal grid size varies from one model to another. Most of the SCMs used the same vertical resolution as their parent GCMs (Table 3). The horizontal grid size used in 2-D CRMs is between 2 and 3 km. The rest of the simulation designs can be found in previous model intercomparison studies such as *Xu et al.* [2002] and *Xie et al.* [2002], as well as in the work of *Xie et al.* [2005].

[21] The simulation starts from the beginning of the period, 1130 UT 15 March, and ends at 2330 UT 19 March of the ARM March 2000 IOP. Details of the observed frontal cloud systems are given in section 3 below.

3. Observational Data and Analysis

3.1. Available Data

[22] The ARM March 2000 IOP covers a 21 day period, starting from 1130 UT 1 March 2000, but only a portion of the IOP is simulated in this study. It is called a cloud IOP because of the abundance of cloud measurements, many of which were not available during earlier IOPs that had been used for model intercomparison studies [*Ghan et al.*, 2000; *Xie et al.*, 2002; *Xu et al.*, 2002]. This IOP provides a useful data set for evaluating cloud microphysics parameterizations in SCMs and CRMs. Specifically, the new measurements include the vertical profiles of cloud liquid water content (LWC) and ice water content (IWC), as well as cloud ice water path from the ARM microbase products [*Miller et al.*, 2004]. Please refer to *Xie et al.* [2005] for a discussion of the uncertainties of these measurements. As in the earlier IOPs, the vertical profiles of cloud hydrometeor frequency, column hydrometeor fraction and cloud liquid water path (CLWP) are available from the Active Remotely Sensed Cloud Layers (ARSCL) data archive [*Clothiaux et al.*, 1999]. Cloud fraction is used in this study, in place of the hydrometeor frequency, which is a single-point measurement at the ARM SGP central facility and includes a contribution from precipitating particles. Traditional mea-

Table 3. A List of Model Levels and Grid Sizes Used in the Intercomparison Study[a]

Model	Model Levels	Horizontal Grid Size, km	Vertical Grid Size Below 100 hPa
CSU SCM	17	-	35–100 hPa
ECHAM5	19	-	10–90 hPa
GFDL	24	-	10–80 hPa
GISS	35	-	10–80 hPa
McRAS	17	-	20–80 hPa
PNNL	24	-	5–90 hPa
SCAM	26	-	15–90 hPa
Scripps	53	-	5–25 hPa
CSU SAM	63	2	13–40 hPa, 100–500 m
ISU	35	3	13–40 hPa, 100–1000 m
UCLA/LaRC	45	2	13–40 hPa, 100–500 m
ARPS/LaRC	50	2	13–40 hPa, 100–600 m

[a]All CRMs are 2-D, oriented on the east-west direction.

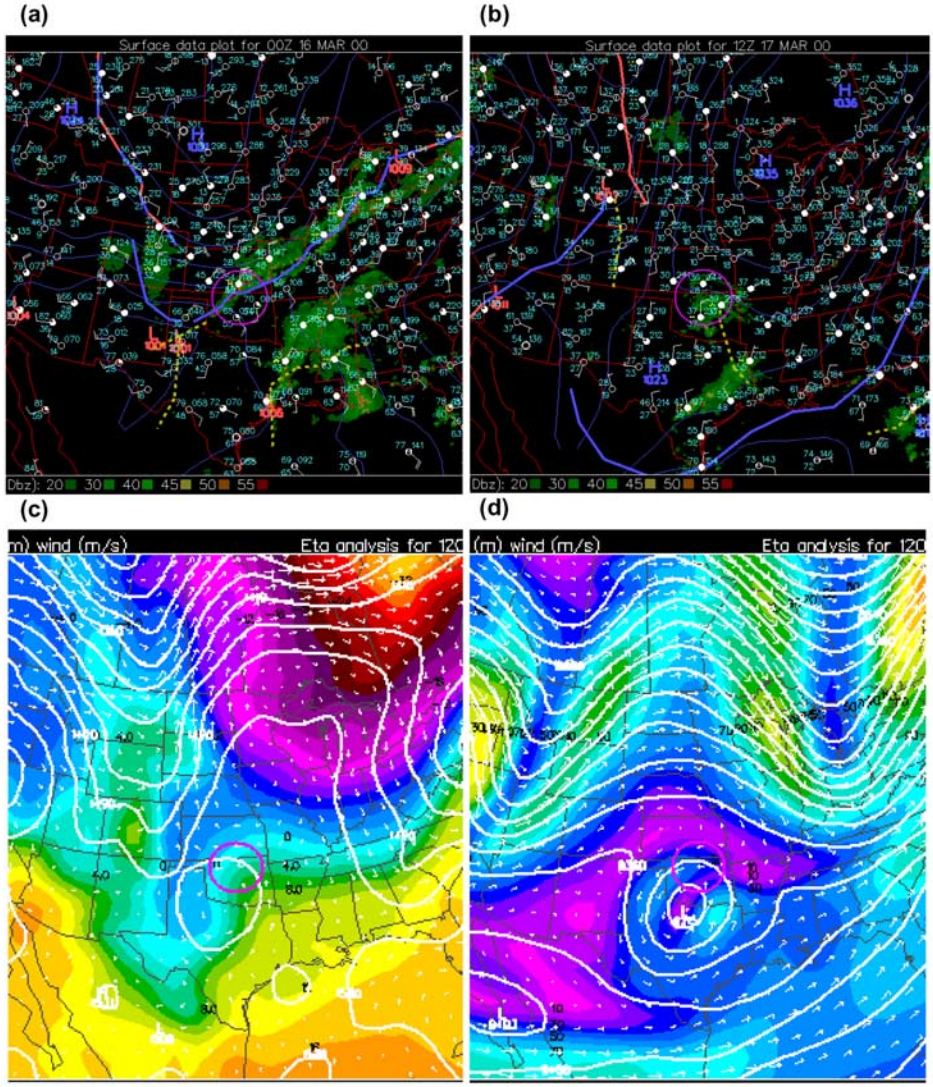

Figure 2. Surface analysis of the continental United States for (a) 0000 UT 16 March 2000 and (b) 1200 UT 17 March 2000 and upper air analysis from the NCEP Eta model, at (c) 850 hPa and (d) 300 hPa, for 1200 UT 17 March 2000. In Figures 2a and 2b the radar reflectivity is denoted on the maps by shaded green areas. Thick dashed lines represent the troughs while the thick solid lines represent fronts. The circles denote the ARM Cloud and Radiation Testbed (CART) domain.

surements such as RH and surface precipitation rate are also valuable for model evaluation.

[23] External data sets that are not a part of the ARM standard data set include the NOAA Geostationary satellite (GOES-8) images provided by Patrick Minnis's group at NASA Langley Research Center, radar images provided by the NOAA National Severe Storm Laboratory, and synoptic analysis maps from the NOAA National Centers for Environmental Prediction's (NCEP) Eta model. All of these are used to provide a comprehensive description of the large-scale synoptic conditions associated with the frontal cloud systems to be modeled in this study.

[24] In order to perform the SCM/CRM simulations, large-scale advective tendencies are needed to drive the models. Balloonborne soundings of winds, temperature and dew point temperature were obtained every 3 hours from the CART central facility located near Lamont, OK (36.61°N, 97.49°W) and from four boundary facilities, which form a domain that is approximately the size of a GCM grid box (about 300 × 370 km^2). The CART domain is roughly labeled by a circle in Figures 2–4. The sounding and wind profiler data, combined with the surface and the top-of-the-atmosphere flux observations, are analyzed over this horizontal domain, using a constrained variational objective analysis method [*Zhang and Lin*, 1997; *Zhang et al.*, 2001]. The final product of this objective analysis is a dynamically and thermodynamically consistent data set, which includes the basic meteorological fields, advective tendencies for driving models and other data for evaluating model performance, with a vertical resolution of 25 hPa for all profile data. However, the horizontal advection of hydrometeors is not available from this analysis because of the lack of adequate measurements.

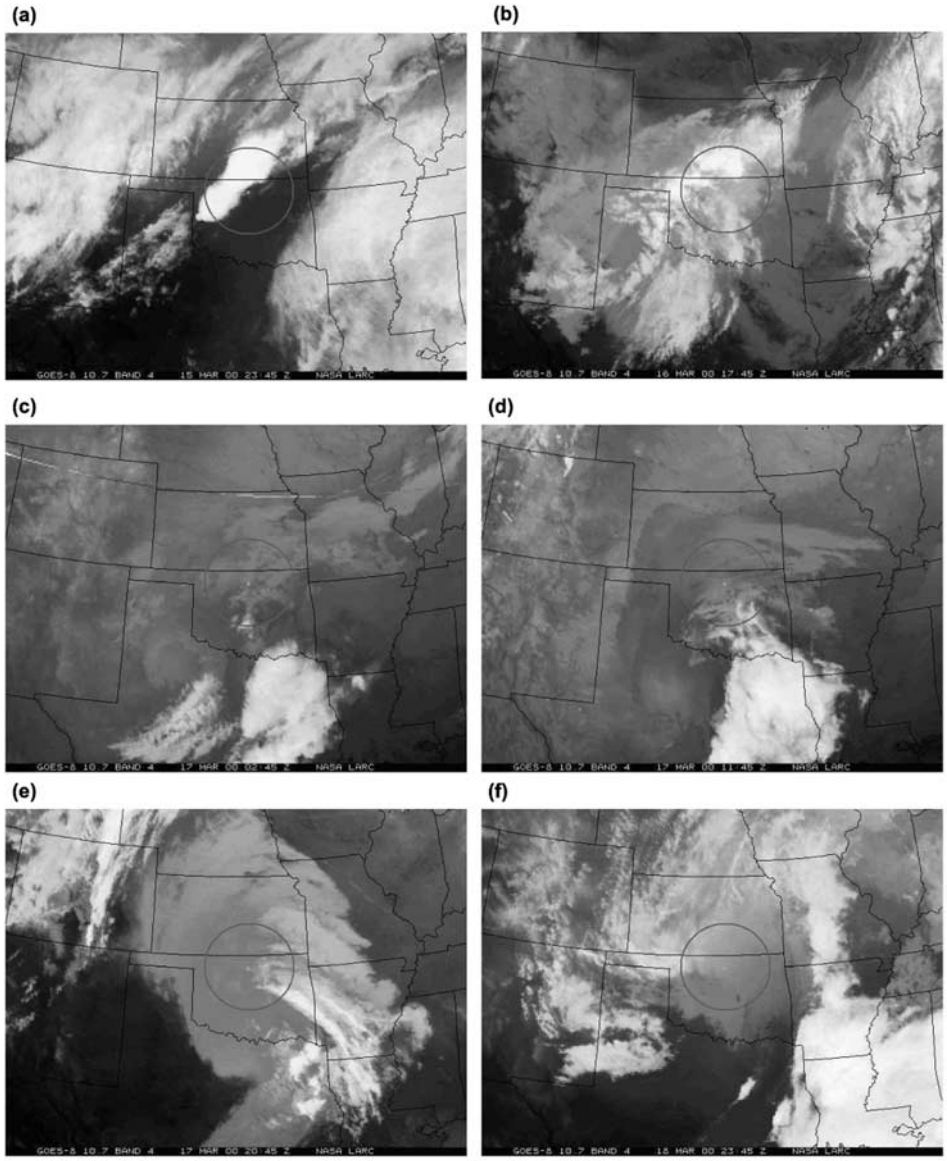

Figure 3. Satellite infrared images for four selected times during the ARM Cloud IOP: (a) at 2345 UT 15 March, (b) 1745 UT 16 March, (c) 0245 UT, (d) 1145 UT, (e) 2045 UT 17 March, and (f) 2330 UT 18 March. The circles indicate the ARM Cloud and Radiation Testbed (CART) domain.

3.2. Synoptic Conditions

[25] The period chosen for this study starts from 1130 UT 15 March and ends at 2330 UT 19 March, with an emphasis on the shallow frontal clouds observed between 0300 UT 17 March and 0600 UT 18 March. Figures 2 and 3 show a few selected times of the surface and upper air analyses from the NCEP Eta model and the GOES-8 satellite images, respectively. This period is characterized by the passage of a cold front through the ARM CART domain at the beginning of this period and frontogenesis associated with a quasi-stationary isolated low pressure center throughout the remainder of this period. The cold front approached the CART domain from the north and passed the northwest corner of the CART domain at 1800 UT 15 March (Figures 2a and 3a). The southerly winds to the east of the low pressure center are associated with massive moisture transport from the Gulf of Mexico at 1200 UT 17 March (Figure 3) and the isolated low pressure center at 300 hPa is located within a large-scale ridge, which is associated with downward motion (Figure 2d).

[26] In the lower troposphere, the continuous advection of cold air from the area northwest of the CART domain and the massive moisture transport from the Gulf of Mexico to the southern part of the CART domain were the main forcing mechanisms of the quasi-stationary front. The shallow cloud systems observed during the period were located over much of the isolated low pressure system (Figures 3c–3f). Occasional deep clouds passed through the CART domain. An upper level trough moved over the domain destroying this stationary system at the end of the period (Figure 3f).

3.3. CART Domain Observations

[27] Radar observations show that all surface precipitation systems that occurred in this period are larger than

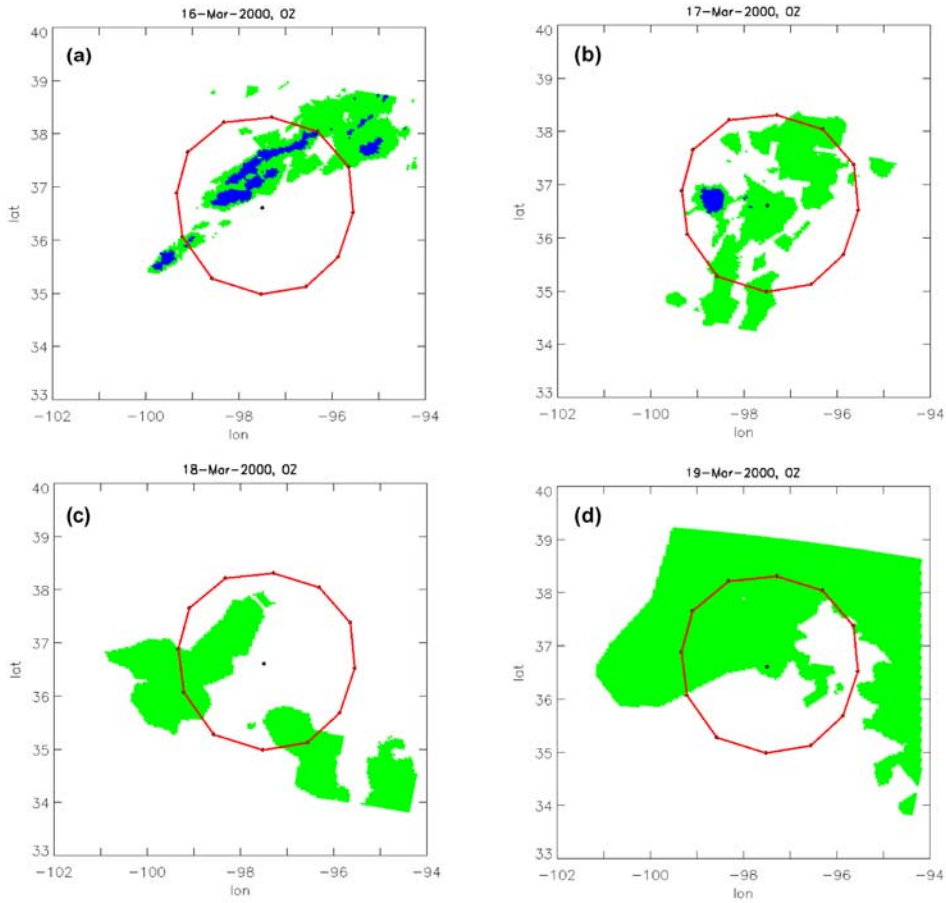

Figure 4. Radar reflectivity maps during the ARM Cloud IOP for four selected times: (a) 0000 UT 16 March, (b) 0000 UT 17 March, (c) 0000 UT 18 March, and (d) 0000 UT 19 March. The circles indicate the ARM Cloud and Radiation Testbed (CART) domain.

the CART domain (Figure 4). This is a feature that is fundamentally different from that of summertime precipitation because summertime precipitation tends to be locally generated inside the domain more often than it is advected into the domain. Strong precipitation was associated with the passage of the cold front at the beginning of this period, while the intensity of precipitation was weaker in the domain for the rest of this period because the precipitation was associated with the shallow frontal cloud systems. On no occasion did the observed precipitation features cover the entire CART domain (Figure 4).

[28] During this period, the temperature and moisture fields in the lower troposphere gradually decreased (Figure 5). The air was warmer (283–288 K) near the surface before the passage of a cold front during the early hours of 16 March. Later on 16 March, the temperature dropped to below 273 K in the lowest 1 km for about 12 hours, when cloud ice/snow was observed. This feature is mentioned because, as described later, model-simulated positive temperature biases as a result of advective warming are high enough that the simulated temperature in the lowest 1 km never drops below 273 K to produce ice clouds in any of the models. The highest water vapor mixing ratio was 9 g kg^{-1} on 15 March. The surface water vapor mixing ratio dropped to 4 g kg^{-1} after the passage of the cold front. It increased to 5 g kg^{-1} between 18 and 19 March.

[29] Figure 6 shows the hydrometeors, cloud fraction and relative humidity during this period. In spite of the low water vapor mixing ratio, the RH is very high in the lower troposphere throughout this period due to the moisture transport from the southerly to the east of the quasi-stationary low pressure center mentioned earlier and in the entire troposphere on 16 and 19 March due to frontogenesis. There is, however, a minimum (~80%) in the lower troposphere on 17 March, which is associated with a strong horizontal advective warming (>20 K day^{-1}; Figure 7c). There is a weak signal of near cloud-free area in the microwavelength millimeter cloud radar (MMCR; *Moran et al.* [1998]) observations of cloud fraction around 1000 UT 17 March (Figure 6c). Satellite images indicate that the areal cloud amount of the CART domain is small at this time (Figure 3d). There was a dry region in the middle and upper troposphere between 17 and 18 March, which corresponds to the nearly clear sky above the shallow frontal clouds (Figure 6c).

[30] It is not surprising that significant variabilities of LWCs were observed with maximum magnitudes exceeding 1 g kg^{-1} (Figure 6a) while the MMCR measurements of cloud fraction showed small variabilities when clouds were

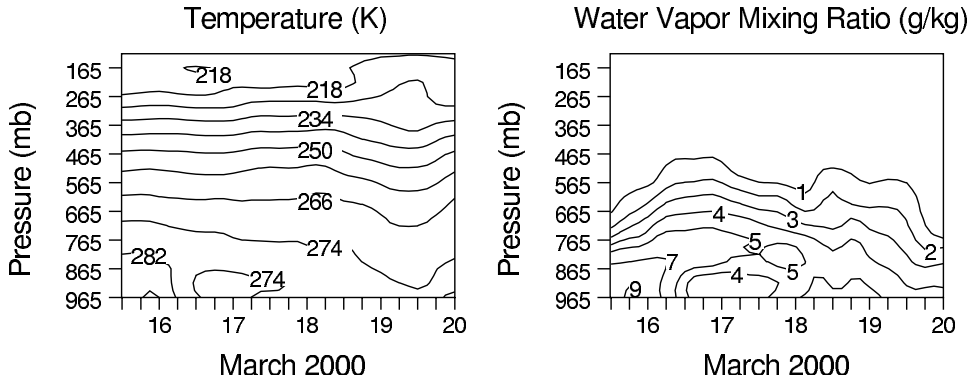

Figure 5. Time-pressure cross section of the observed temperature and moisture for a short period during the March 2000 intensive operational period (IOP).

present (Figure 6c). There are multiple peaks in the observations of LWC on 16 March and 18 March. The magnitudes also vary greatly when only shallow cloud systems were observed on 17 and 18 March. Another important feature worth noticing is that the peak magnitudes of both LWC and cloud fraction (Figures 6a and 6c) extend all way down to the surface, which may suggest that the retrieved LWC includes some rainwater content at times because precipitation is present during this period (Figure 8). Precipitation peaks were observed at 0300 UT 16 March, 1500 UT 17 March and 1800 UT 18 March. Each of these peaks is associated with significant growth in the vertical extent of the clouds (Figure 6c). Retrieval procedures have been well tested on thin nonprecipitating clouds, but not on thick precipitating clouds for this IOP [*Dong and Mace*, 2003]. Some of the retrieved LWC and IWC features

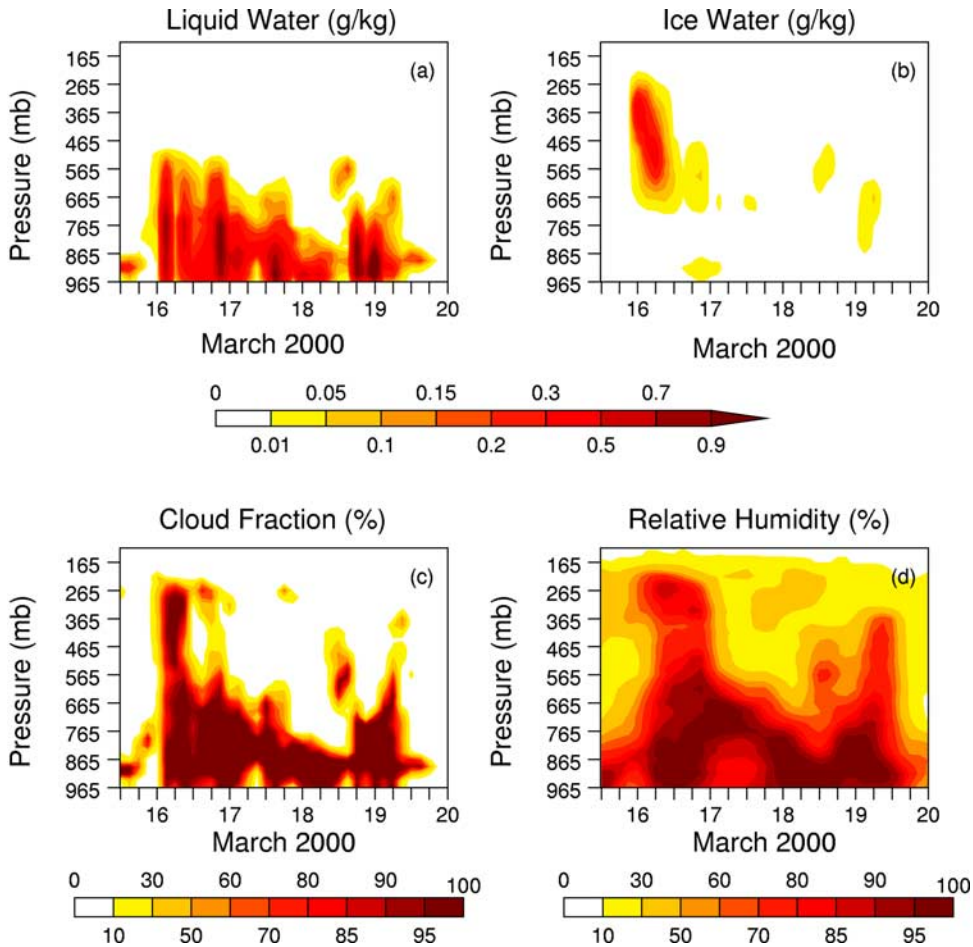

Figure 6. Time-pressure cross section of the observed (a) liquid water content, (b) ice water content, (c) cloud fraction, and (d) relative humidity for a short period during the March 2000 intensive operational period (IOP).

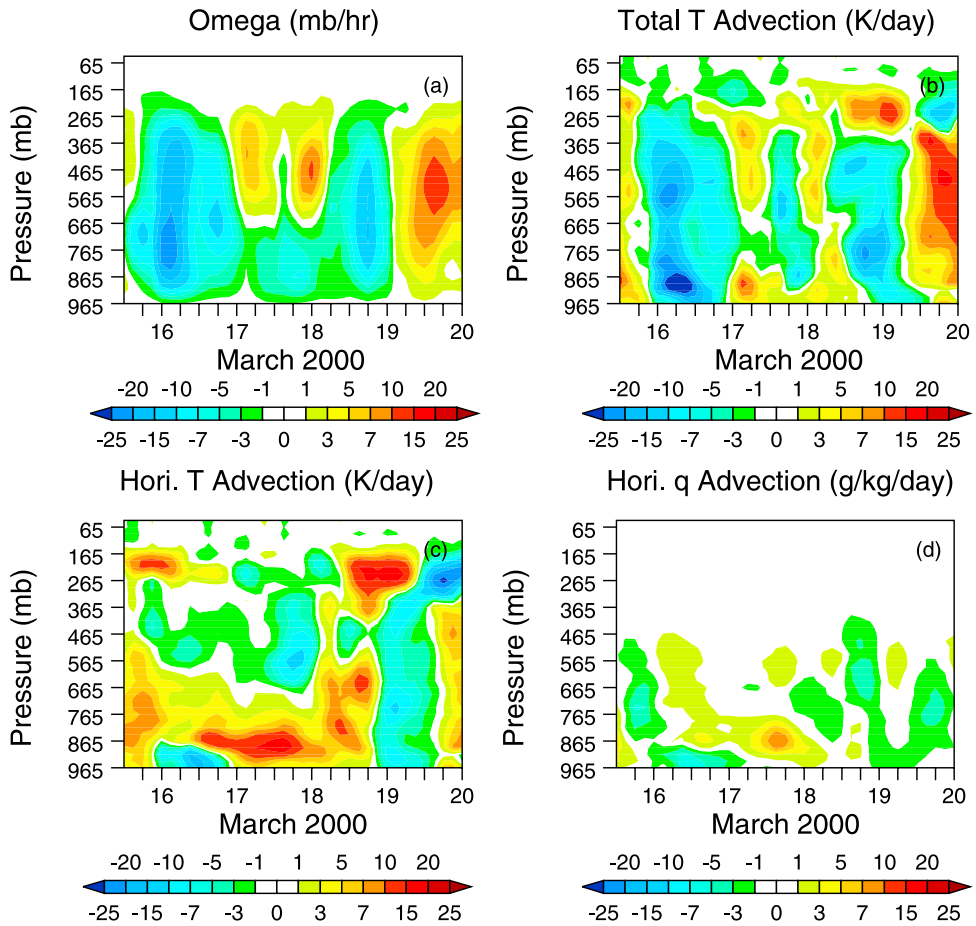

Figure 7. Time-pressure cross section of (a) large-scale vertical velocity in pressure coordinate, (b) large-scale total advective heating rate, (c) large-scale horizontal advective heating rates, and (d) large-scale horizontal advective moistening rate for a short period of the March 2000 intensive operational period (IOP).

should, therefore, be treated with caution. Cloud ice was only sporadically present during this period because most of the observed cloud systems were shallow, except for the passage of the cold front on 16 March and occasional passage of upper-level clouds in the later portion of this period (Figure 6b). The maximum IWC magnitudes were less than 0.1 g kg^{-1} for all of this period except for the IWC associated with the deep cold front on 16 March.

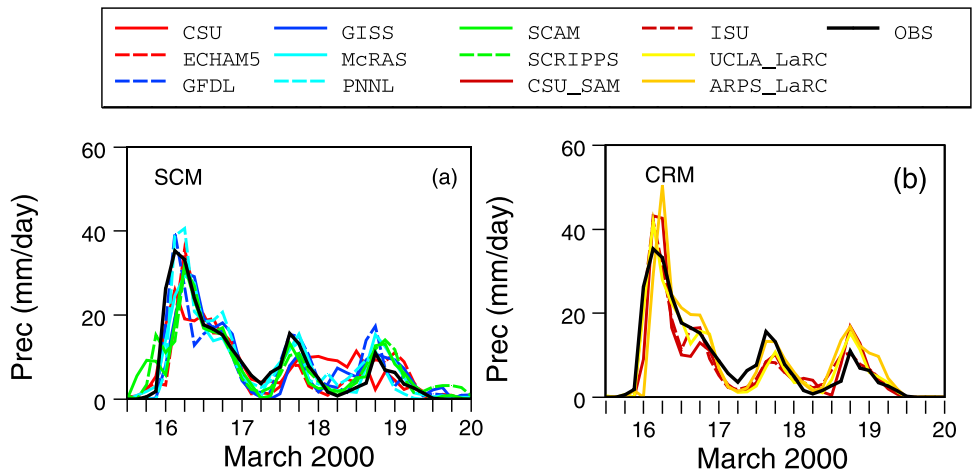

Figure 8. Time series of surface precipitation rates simulated by (a) SCMs and (b) CRMs. The observed surface precipitation rates are denoted by solid black curves.

3.4. Large-Scale Forcing for Driving the Model Simulations

[31] The large-scale vertical velocity has a strong upward motion (-20 hPa hr^{-1} or lower) during the passage of the cold front on 16 March and a moderate upward motion (between -10 and -20 hPa hr^{-1}) in the later hours of 18 March. Weak subsidence is present in the upper troposphere on 17 March and in the entire troposphere on 19 March. There is a weak peak of upward motion in the middle and upper troposphere around 1500 UT 17 March. Satellite cloud images (Figure 3) indicate that this might be the result of averaging over subsidence and strong ascending bands embedded in the cloud system (Figure 7a). The total advective tendency thus has a significant amount of cooling (Figure 7b). This feature is a source of significant model biases discussed in section 4.

[32] The horizontal advection of potential temperature has a very different structure compared to that of the large-scale vertical motion (Figure 7c). There is a thick layer in the lower troposphere that is associated with advective warming between 15 and 18 March, with a maximum strength of greater than 20 K day^{-1} at 850 hPa on 17 March. Horizontal advective cooling occurs below 900 hPa between the late hours of 15 March and most of 16 March, which is associated with the passage of the cold front. Advective drying occurs in the middle and upper troposphere before the passage of the cold front and in the lower troposphere on 16 March (Figure 7d). There is a layer of advective moistening in the observed shallow cloud layer on 17 March and it lasts until the early hours of 18 March. Advective drying is also pronounced in the last two days of the period.

4. Results of Intercomparison

[33] In this section, the performance of eight SCMs and four CRMs in simulating shallow and deep frontal clouds is examined, with an emphasis on the simulations of shallow frontal (SF) clouds. A 27 hour period lasting from 0300 UT 17 March to 0600 UT 18 March (hereafter, the SF period) is chosen because observed shallow frontal cloud systems were most persistent. The observed upper troposphere was very dry during this period, which was not favorable for the formation of deep frontal clouds (Figures 3c and 6d). Results from the CRM and SCM simulations will be discussed below. Specific questions to be addressed are:

[34] 1. To what extent do the CRMs and SCMs realistically simulate the vertical profiles of cloud fraction and cloud microphysical properties?

[35] 2. What are the physical causes of the biases in the shallow frontal clouds simulated by the CRMs and SCMs?

[36] 3. What are the main reasons for the intermodel differences?

[37] 4. Do the CRMs perform better than the SCMs for the shallow frontal cloud simulations?The first question and part of the second question will be addressed in sections 4.1 and 4.2 while the last three questions will be addressed in section 4.3. A summary will be given in section 4.4.

[38] Before the model results are presented, some cautions are made here regarding the observational data of cloud fraction and cloud microphysical profiles and the forcing data. First, the ARSCL cloud tops shown in Figure 6c represent point measurements and underestimate the actual cloud tops when the radar signal is contaminated by rain. For the same reasons, ARSCL clouds in the lowest 100 hPa near the surface may not be accurate. Second, the vertical structure of the imposed large-scale vertical velocity data, with downward motion in the upper troposphere and upward motion in the lower troposphere during the SF period, as shown in Figure 7a, has uncertainties in accurately resolving the transition altitude, which will have implications regarding the accurate simulations of cloud top heights in the models. With these two caveats in mind, the following gross features will be sought in the models: (1) the reduction of upper tropospheric RHs and cloud amounts at the beginning of 17 March; (2) the low-tropospheric clouds as depicted in the ARSCL and satellite data during the SF period (Figure 3); (3) the transition of low-level clouds to middle- and high-level clouds at the end of 18 March; (4) the subsequent dissipation of all clouds at the end of 19 March (Figure 6c); and (5) the associated cloud microphysical properties during this period (Figures 6a and 6b).

4.1. CRM Simulations

[39] To realistically simulate the vertical profiles of cloud fraction and microphysical properties, the RH field must be realistically simulated. All four CRMs simulate the vertical structures of RHs well during the first 36 hours of the integration, including the reduction of upper tropospheric RH at the beginning of 17 March (Figure 9). During the last three days of the integration, RHs in the models differ greatly, however. RHs are slightly higher than observed in the CSU and UCLA/LaRC CRMs, but significantly higher in the ISU CRM and significantly lower in the upper troposphere of the ARPS/LaRC CRM and near the surface layer of the ISU CRM. Both the CSU and UCLA/LaRC CRMs reproduce the dry middle/upper troposphere on 17 March somewhat well although the RH starts to increase in the late hours of 17 March, due to the imposed advective cooling (Figure 7). The mean RH profiles for the SF period show various degrees of overestimates in the upper tropospheric RHs among the CRMs (Figure 10c). The poor simulations of the upper tropospheric RHs are likely related to the dynamics (and/or numerics) of the ISU and ARPS/LaRC CRMs because no clouds are simulated above 400 hPa starting from 17 March. These two CRMs use compressible dynamics, while the CSU and UCLA/LaRC CRMs use anelastic dynamics. The numerical schemes with anelastic dynamics have more accurate conservation properties. However, overestimates of middle tropospheric RHs in all CRMs may be attributed to inaccurate forcing data, the second caveat given at the beginning of this section.

[40] The deep frontal clouds are simulated in all four CRMs on 16 March (Figure 11) when the RH fields are well simulated. The magnitudes of the cloud fractions are underestimated, however, particularly in the middle troposphere and the early phase of the frontal passage. This is consistent with the results shown in the work of *Xie et al.* [2005]. This result is expected because saturation cannot be produced at all grid points of the CRM domain when convective circulations, instead of mesoscale frontal circulations, are

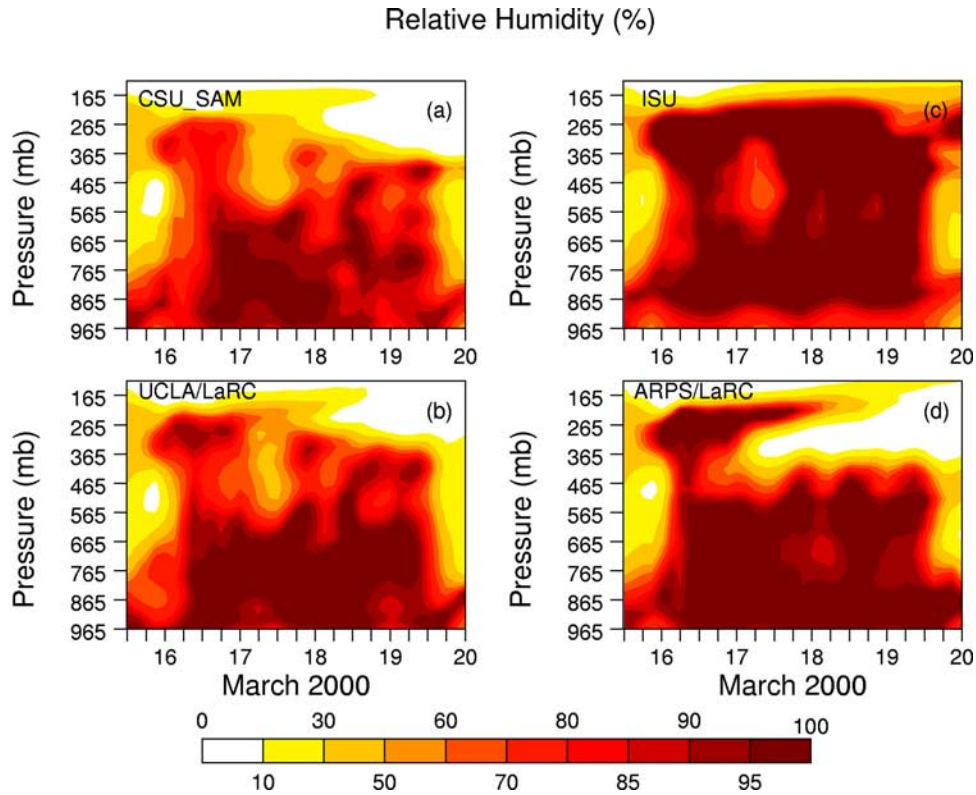

Figure 9. Time-pressure cross section of the relative humidity simulated by CRMs: (a) CSU SAM, (b) UCLA/LaRC, (c) ISU, and (d) ARPS/LaRC.

produced due to the imposed strong large-scale forcing at the early hours of the frontal passage (Figures 7a and 7b). This is related to deficiencies in the 2-D configuration of CRMs for simulating frontal clouds discussed in section 1; i.e., 3-D CRMs are expected to perform better. Induced subsidence by convective circulations is largely responsible for the underestimate of cloud fraction. Another factor that may be associated with the underestimate is that the observed cloud fraction from the MMCR includes a contribution from precipitating hydrometeors while the CRM-diagnosed cloud fraction includes those grids with cloud condensate only. An underestimate of cloud fraction would, thus, be expected even if all CRMs were perfect and the single-point measurements were representative of the areal average.

[41] The shallow frontal clouds during the SF period are generally well simulated although they are underestimated to various degrees by all four CRMs (Figure 11) in the sense that no clouds are simulated in the upper troposphere in spite of the large overestimate of RHs there (Figure 10c). The agreement between the CSU and UCLA/LaRC simulations with the observations is remarkable because the gradual increase of cloud fraction and the gradual decrease of cloud base and top heights are well reproduced during the SF period. The satellite observations indicate that column cloud amount is far less than overcast at the beginning of the SF period (Figures 3c and 3d). So, neither the CSU nor UCLA/CSU CRM greatly underestimates the cloud amount, compared to the GOES observations. However, the ISU and ARPS/LaRC CRMs have difficulties in capturing the general characteristics of the observed shallow clouds during the SF period. This may also be attributable to the differences in the dynamical framework of the CRMs mentioned earlier.

[42] Excessively large advective heating may produce the cloud-free layer in the lowest 100 hPa at the beginning of the SF period that are more pronounced than in the MMCR measurements (Figure 6c). Consequently, the mean cloud fraction and LWC profiles over the SF period show large underestimates in the lowest 125 hPa, compared to the MMCR observations, although the mean cloud fractions agree with the MMCR observations rather well above 800 hPa in both the CSU SAM and UCLA/LaRC CRMs (Figures 11a, 11b, and 12a).

[43] A noticeable feature appearing in Figure 11 is that a secondary maximum in cloud fraction is slightly tilted with height (above 700 hPa) between 1200 and 2000 UT 17 March except for the ISU CRM. However, the observed cloud fraction shows no such vertical phase tilting (Figure 6c). This tilted maximum center is associated with individual convective cells that slowly develop above the shallow cloud layer. Another weak phase tilting feature is also simulated in all four CRMs between 18 and 19 March, especially above 500 hPa. This may be related to the lack of horizontal advective forcing of condensate, since models are forced to generate clouds slowly due to the small magnitudes of the imposed advective forcings in the upper troposphere (Figure 7).

[44] The CRMs seem to quantitatively simulate the vertical extents of LWC and IWC (Figures 13 and 14), compared to the observations (Figures 6a and 6b). This is

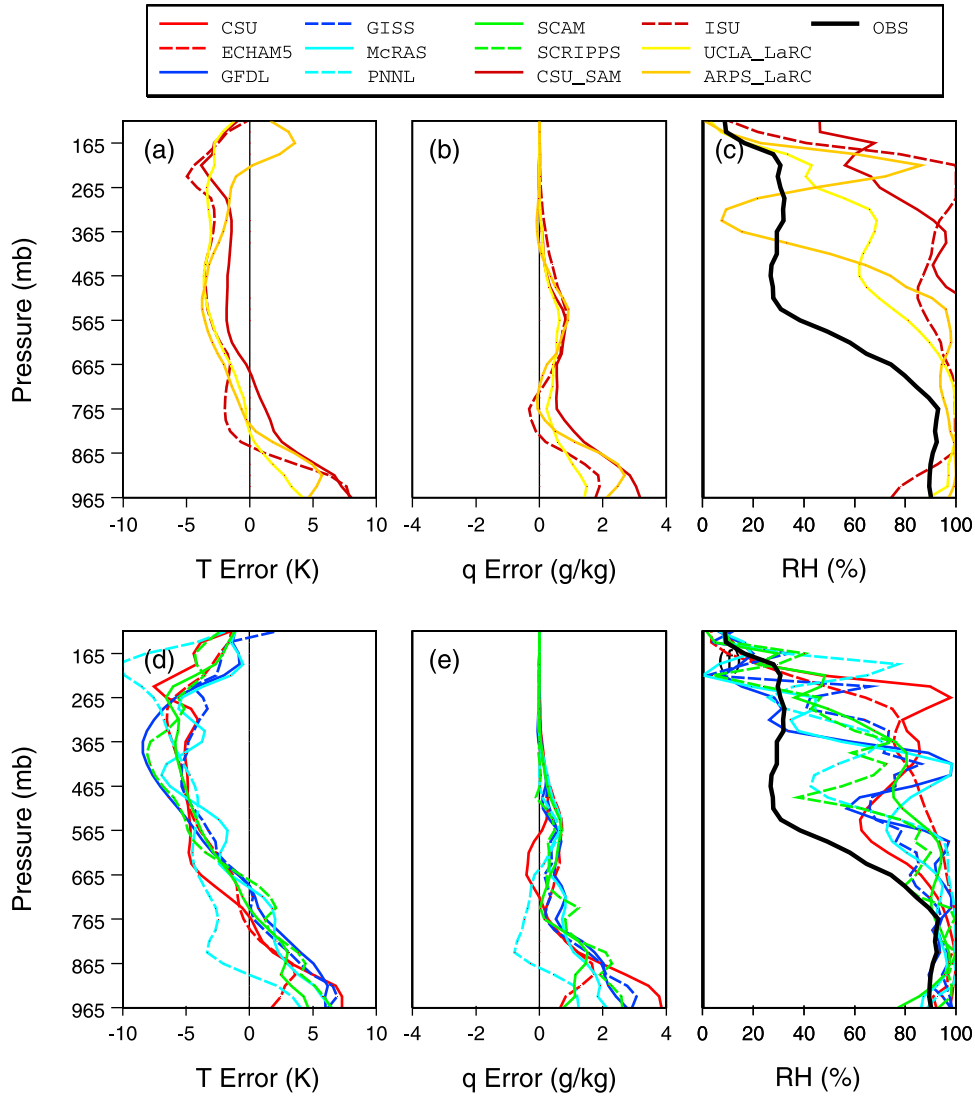

Figure 10. Vertical profiles of averaged temperature and water vapor mixing ratio deviations from the observed and the simulated and observed averaged relative humidity from (a–c) CRMs and (d–f) SCMs. The averaging period is from 0300 UT 17 March to 0600 UT 18 March.

an encouraging result although there are large uncertainties in the observed LWC and IWC. However, the magnitudes of LWCs are underestimated in all CRMs, especially during the passage of the cold fronts on 15 and 18 March. The underestimate of the magnitudes can be explained by the deficiencies in cloud microphysics parameterizations and the lack of horizontal advection of hydrometeors into the domain. Assuming a uniform advection with a wind speed of 10 m s^{-1} over a 300 km wide domain and an advected hydrometeor mixing ratio of 1 g kg^{-1}, the advective tendency will be 0.3×10^{-4} g kg^{-1} s^{-1}. The change of hydrometeor mixing ratio over a 3 hour period will be 0.36 g kg^{-1}. This is comparable to the magnitude of the underestimate shown in Figures 13 and 14. However, the lack of horizontal advection of hydrometeor out of the domain prolongs the life cycle of clouds until large-scale subsidence destroys the clouds. The production of clouds from this ballpark estimate of hydrometeor advection is much greater than that due to some microphysical processes, such as the autoconversion rates shown in Figure 1.

4.2. Overall Results of SCM Simulations

[45] Figure 15 shows that high RHs in the lower troposphere are simulated throughout the four and a half day period by all SCMs. High RHs in the middle and upper troposphere are associated with the passage of the cold fronts on 16 and 18 March. The simulated RHs are slightly lower than observed at the end of the integration. There are a few features that do not agree well with observations. For example, the low RHs above the shallow cloud layer, as in the CRMs, last for a much shorter time and have a smaller vertical extent in all SCMs and the upper troposphere is much more moist than in the observations.

[46] The overestimate of RHs during the SF period is related to the higher tops of the shallow clouds simulated by most of the SCMs. Another contribution to the overestimate is that the simulated life cycles of the 16 March frontal

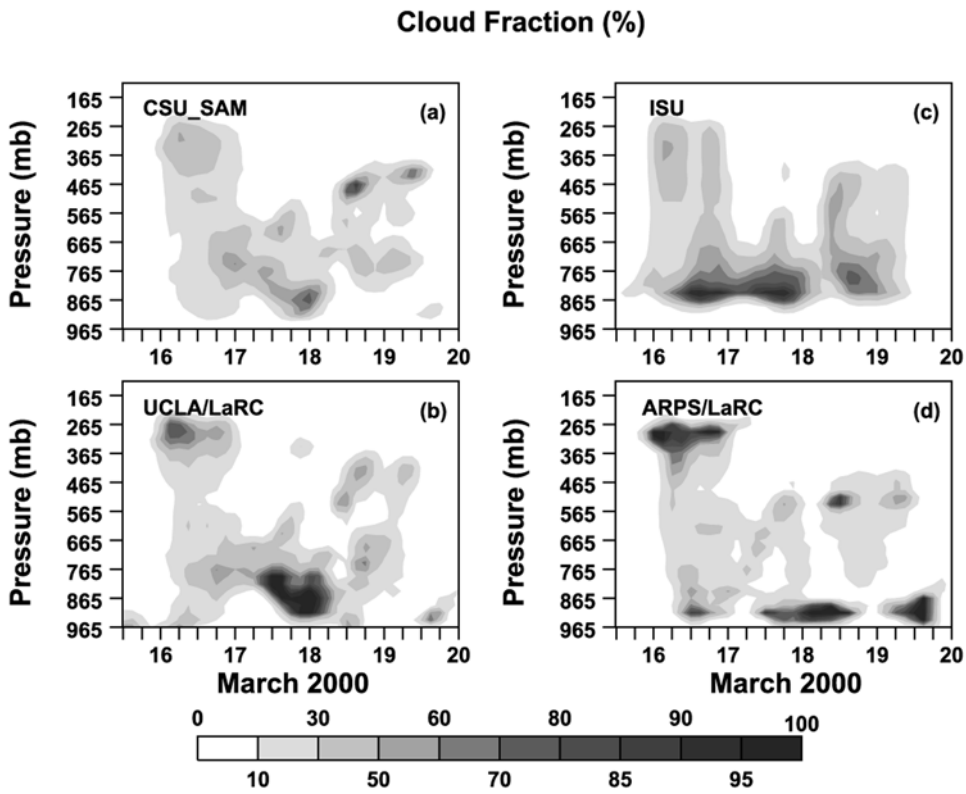

Figure 11. Time-pressure cross section of the cloud fractions simulated by CRMs: (a) CSU SAM, (b) UCLA/LaRC, (c) ISU, and (d) ARPS/LaRC.

clouds are longer than those observed in some SCMs (Figure 16). In some SCMs (e.g., McRAS), the high RHs around 400 hPa are associated with the detrainment of ice from their cumulus parameterization schemes, which moistens the environment and results in a thin cloud layer. Although cumulus convection was not observed, the cumulus parameterization is triggered in the McRAS SCM simulation for this period. The longer life cycles of the 16 March frontal clouds are related to the lack of horizontal advection of condensate out of the CART domain. Subsidence typically follows the horizontal removal of hydrometeors. The lack of such a dissipation process prolongs the life cycles of these clouds past the time when the observed frontal clouds moved out of the domain.

[47] The ice clouds observed near the surface around 0000 UT 17 March (Figure 6b) are not simulated in any of the SCMs (Figures 17 and 18), due to large positive temperature biases there (Figure 19d). Another interesting result appearing in Figure 17 is that the maximum LWC center tilts slightly with height around 0000 UT 18 March in most SCMs, especially in the ECHAM5, SCAM, PNNL and GFDL SCMs, which is similar to the tilt seen in the cloud fraction simulated by all four CRMs. This weak tilt is largely absent in the cloud fraction simulated by SCMs (Figure 16). This feature is, however, also pronounced for the simulated deep frontal clouds on 16 March. Because the magnitudes of LWC are underestimated, it is not clear that this tilt also occurs in the McRAS and Scripps SCMs. As discussed in section 4.1, this tilt feature is likely related to the lack of horizontal advection of hydrometeors.

[48] Additional intermodel differences in the simulation of deep frontal clouds are briefly mentioned here. Please refer to *Xie et al.* [2005] for further discussion. One difference is the lack of middle-level clouds on 16 March in both the ECHAM5 and SCAM SCMs. That is, the transition between liquid- and ice-phase clouds is not well treated. Some conversion processes from condensate to precipitation should be examined in these two SCMs. Another difference is that the lack of IWCs simulated by most SCMs except for the GFDL and GISS SCMs when deep frontal clouds were observed on 16 March (Figure 18). This suggests that the representation of ice-phase clouds is very poor in most of the SCMs, compared to the CRMs (Figures 12 and 14).

4.3. SCM Simulations of Shallow Frontal Clouds

[49] The following discussion of the SCM results will be focused on the shallow frontal clouds during the SF period (Figures 10 and 12) in order to address the specific questions formulated at the beginning of section 4. The mean profiles over the SF period will be extensively examined for this discussion. It is noted that shallow clouds are simulated in all SCMs (Figure 12d). The CSU SCM simulates a nearly perfect mean profile of cloud amount between 565 hPa and the surface without using a fractional cloudiness parameterization (Table 1). Significant differences in the vertical extent and temporal evolution are seen among the models and with the data, however (Figure 16). The observed cloud fraction averaged over the SF period extends from the surface to 565 hPa with a maximum of nearly 100% near

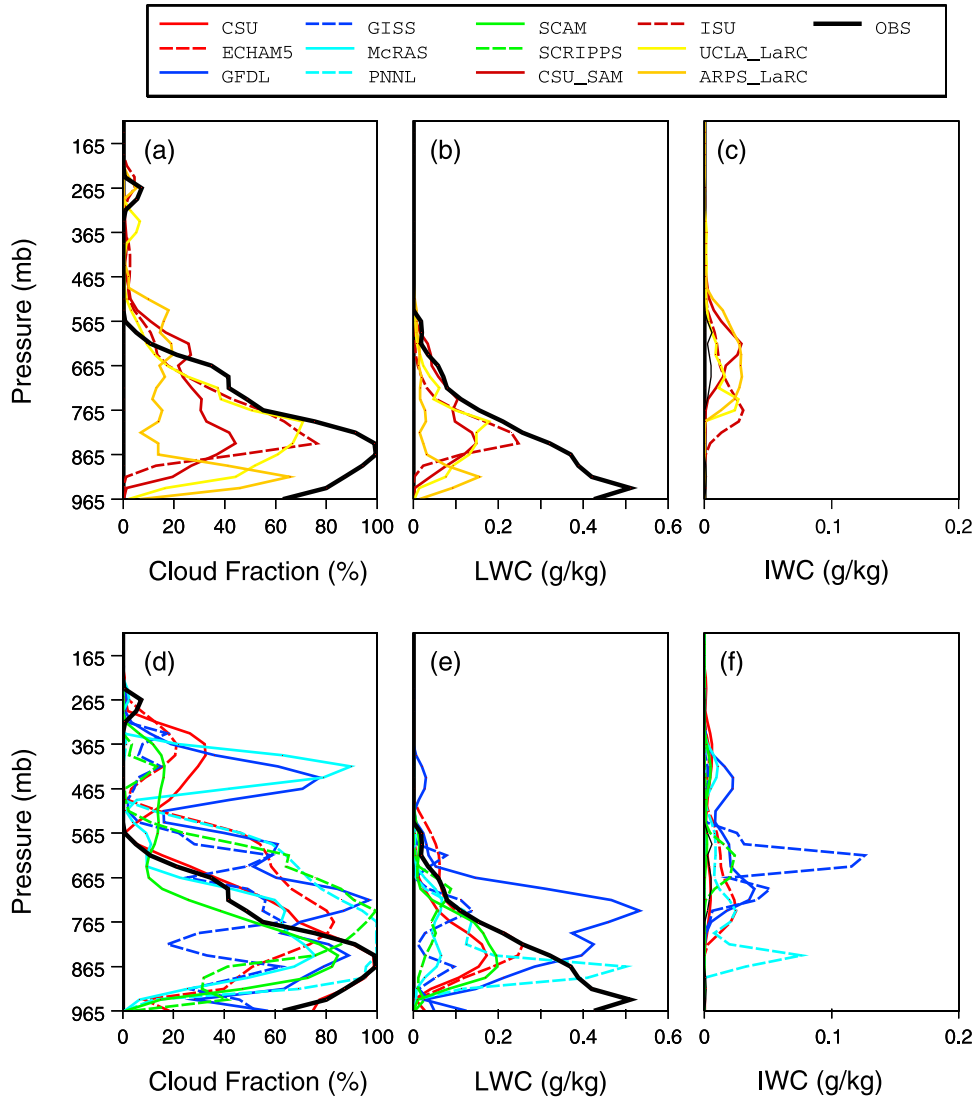

Figure 12. Vertical profiles of simulated and observed averaged cloud fraction, cloud liquid water content, and cloud ice water content from (a–c) CRMs and (d–f) SCMs. The averaging period is from 0300 UT 17 March to 0600 UT 18 March.

865 hPa. The observed cloud fraction is zero between 565 and 285 hPa. The cloud fraction is about 5% near 265 hPa. The MMCR observations only indicate the existence of shallow frontal clouds at the central facility of the CART during the SF period although satellite observations show the presence of high-level clouds in the southern and eastern parts of the SGP domain (Figures 3c–3e). Judging from the satellite cloud images, it can be concluded that the majority of the SGP domain might be still under the influence of downward motion in the upper troposphere at that time while the southeast corner of the domain was undergoing upward motion. It is expected that the models may produce more middle- and high-level clouds during the SF period than the MMCR observations because of the prescribed upward motion and advective cooling that peaked around 1800 UT 17 March (Figure 7b).

[50] All SCMs are somewhat successful in simulating the observed cloud fractions between the surface and 765 hPa except that the GISS SCM significantly underestimates the cloud fraction there. In the lowest 125 hPa, all models underestimate the cloud fraction except for the CSU SCM (Figure 12d). This is, as discussed in section 4.1, possibly due to the inclusion of rainwater in the MMCR measurements and the presence of excessive advective heating at the beginning of the SF period. The major discrepancies in the simulations are the excessive cloud amounts between 765 hPa and 500 hPa simulated by all SCMs, except for the CSU, McRAS and SCAM SCMs, and large estimates (>70%) above 500 hPa in the McRAS and GFDL SCMs and small estimates (10–30%) above 500 hPa in the CSU, ECHAM5, SCAM, GISS and Scripps SCMs (Figures 12d and 16). These discrepancies will be explained separately below.

[51] Why are there such large differences in the SCMs in simulating the observed shallow frontal clouds? Given that the same large-scale forcings are imposed to all models and there is a lack of cumulus convection, cloud microphysics schemes must be responsible for these differences. Within the shallow frontal cloud layer (below 700 hPa), some intermodel differences in the simulated cloud fraction and

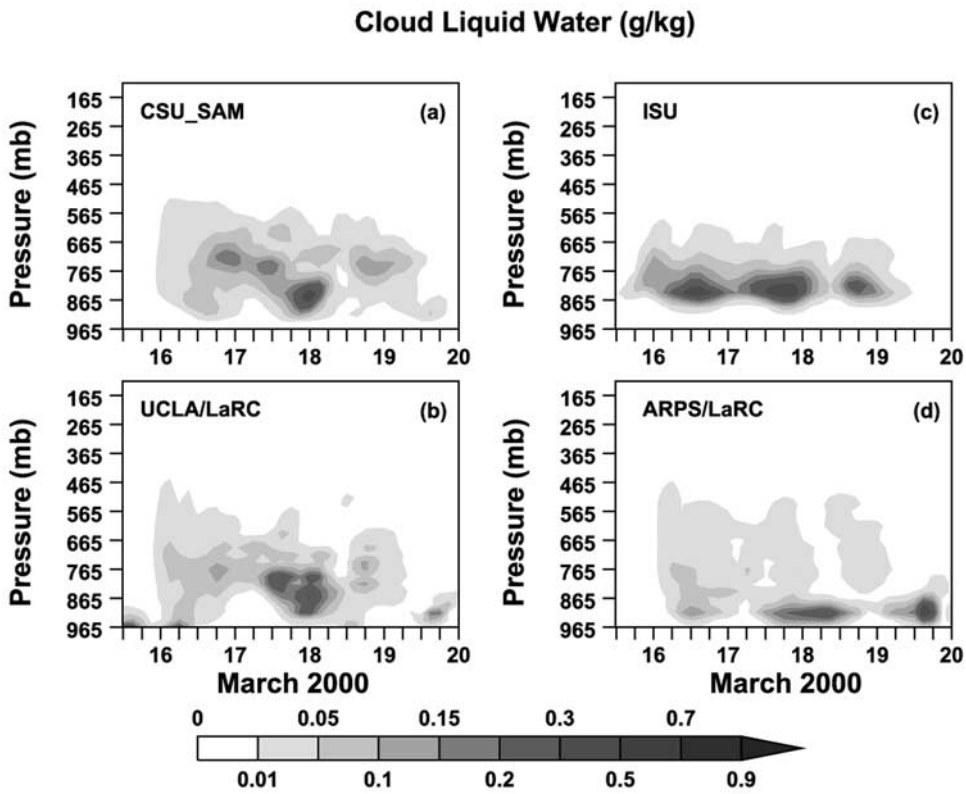

Figure 13. Time-pressure cross section of the cloud liquid water content simulated by CRMs: (a) CSU SAM, (b) UCLA/LaRC, (c) ISU, and (d) ARPS/LaRC.

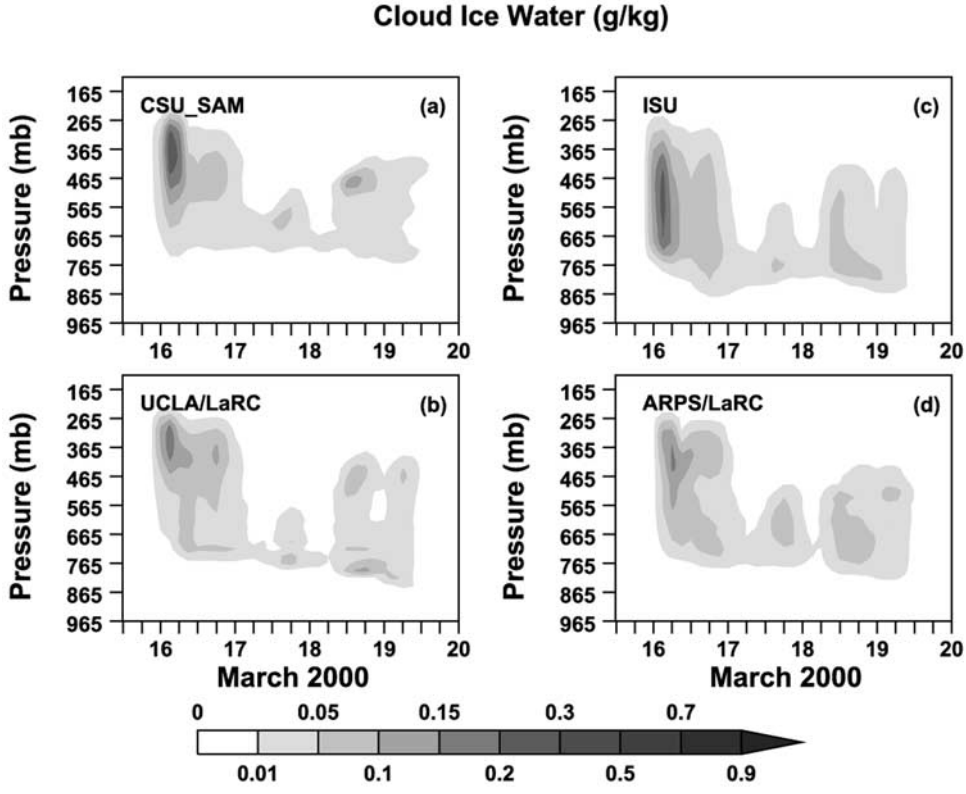

Figure 14. Time-pressure cross section of the cloud ice water content simulated by CRMs: (a) CSU SAM, (b) UCLA/LaRC, (c) ISU, and (d) ARPS/LaRC.

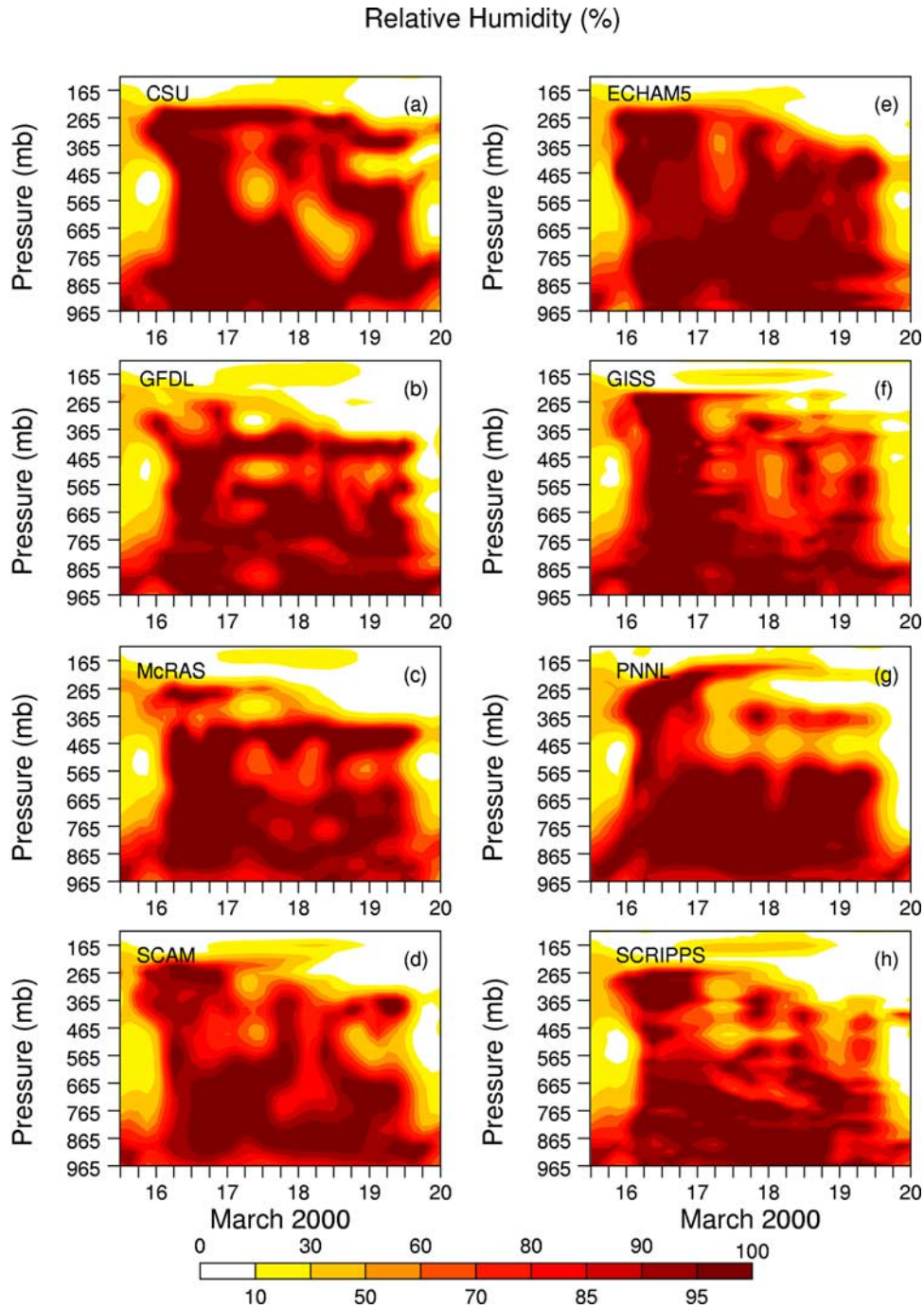

Figure 15. Time-pressure cross section of the relative humidity simulated by SCMs: (a) CSU, (b) GFDL, (c) McRAS, (d) SCAM, (e) ECHAM5, (f) GISS, (g) PNNL, and (h) Scripps.

LWC can be seen in Figures 12d and 12e. Some of these differences can be explained by the different formulations of the microphysical process such as cloud formation/dissipation processes and the autoconversion processes discussed in section 2 (Table 2; Figure 1). For example, the GISS, McRAS and Scripps SCMs, which adopt the Sundqvist-type autoconversion formulation, simulate very small amounts of LWC in the layer between the surface and 700 hPa, compared to the CSU, ECHAM5, SCAM, PNNL and GFDL SCMs which use other schemes. However, the CSU and SCAM results may not be solely explained by the autoconversion process because it is offset by other microphysical processes. Nevertheless, these results may suggest that the Sundqvist formula may cause unrealistically small amounts of LWC to be simulated due to the large autoconversion rates for small cloud water mixing ratios (<1 g kg^{-1}). Results shown in Figure 17 may further support this assertion. The LWC and cloud fraction seem to be less underestimated in the ECHAM5, GFDL, PNNL and SCAM SCMs with formulations of autoconversion that have either higher threshold mixing ratios or smaller autoconversion rates. The higher thresholds suppress nearly all autoconversion. The peak cloud fraction in the GFDL SCM is related to the lack of cloud dissipation process in the cloud scheme

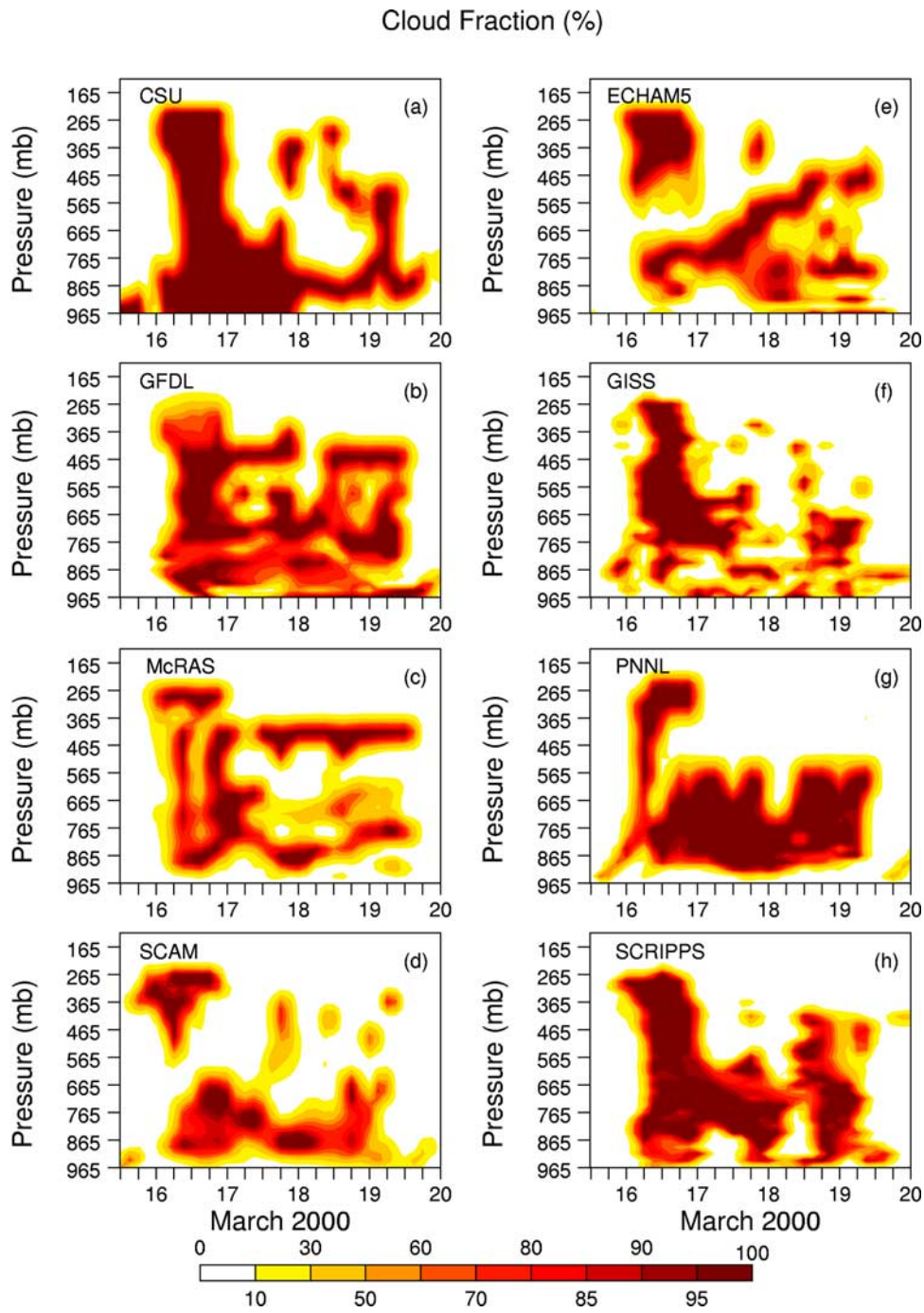

Figure 16. Time-pressure cross section of the cloud fractions simulated by SCMs: (a) CSU, (b) GFDL, (c) McRAS, (d) SCAM, (e) ECHAM5, (f) GISS, (g) PNNL, and (h) Scripps.

of *Tiedtke* [1993]. Despite a good simulation of cloud fraction, which is diagnosed from a small threshold on the sum of LWC and IWC, both the LWC and IWC are underestimated in the CSU SCM. This is related to the small autoconversion threshold that is used to compensate for the lack of a fractional cloudiness parameterization.

[52] Why do some SCMs produce excessive cloud amounts above 500 hPa in contrast to all CRMs even though the RHs are overestimated in both types of models during the SF period (Figure 10)? There are several possible explanations. First, the imposed domain-averaged large-scale tendencies have been averaged over both subsidence regions and ascending bands. The imposed large-scale subsidence was not strong enough to suppress the residual middle-level clouds from the early deep frontal cloud system in all SCMs (Figure 16). However, clouds are suppressed in the CRMs because of explicitly resolved cloud-scale dynamics.

[53] Second, there is a decoupling between cloud condensate and cloud fraction in almost all SCM parameterizations (except for CSU and ECHAM5) so that the large amounts of cloud fraction are diagnosed as a result of overestimated RHs while the simulated cloud condensate amount is almost nonexistent. This explanation is supported

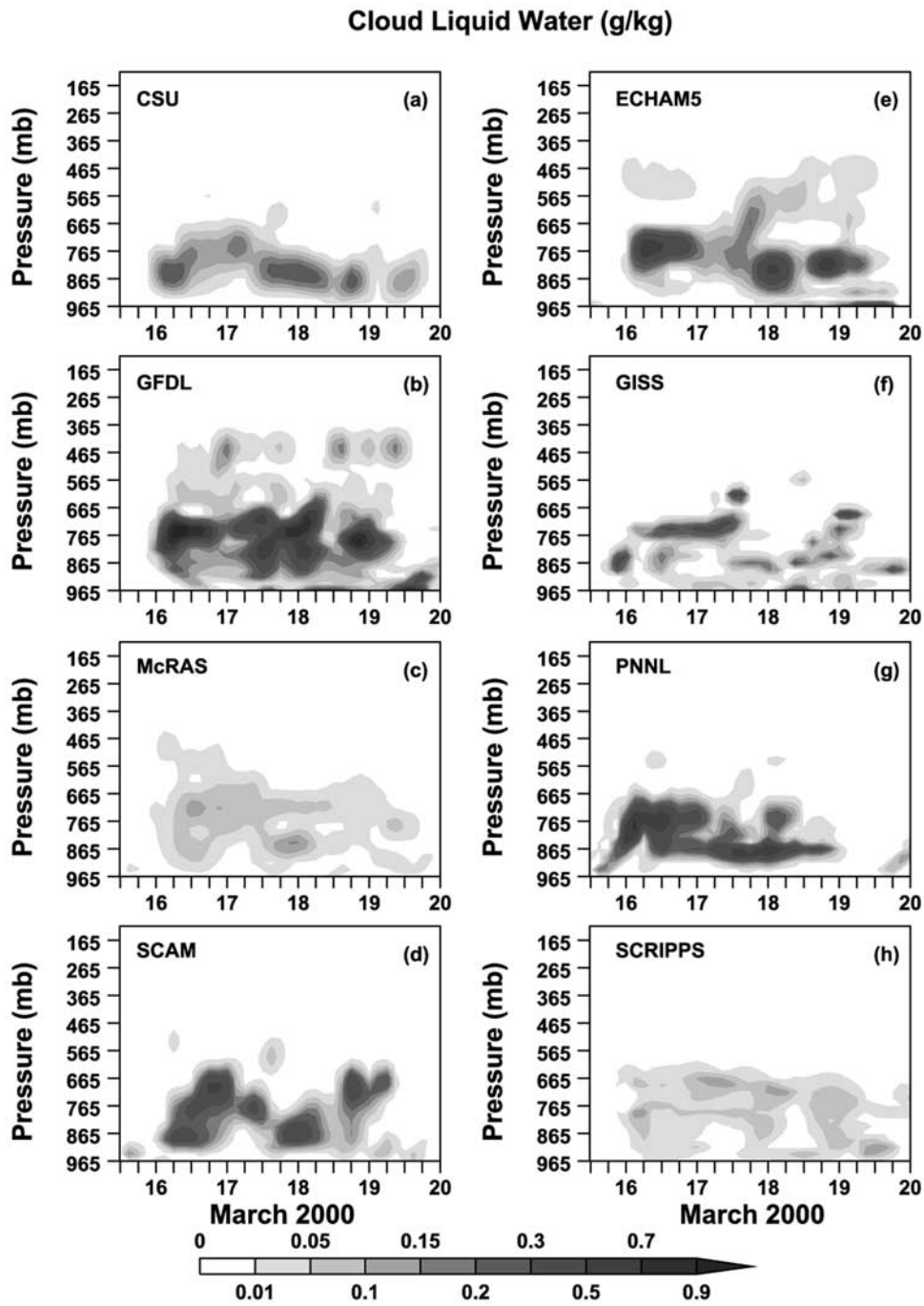

Figure 17. Time-pressure cross section of the cloud liquid water content simulated by SCMs: (a) CSU, (b) GFDL, (c) McRAS, (d) SCAM, (e) ECHAM5, (f) GISS, (g) PNNL, and (h) Scripps.

by the results shown in Figures 12e and 12f because both the simulated LWCs and IWCs are very small (<0.1 g kg^{-1}) above 500 hPa. This lack of a coupling between cloud condensate and cloud fraction except for the ECHAM5 SCM is related to the RH-based parameterizations of cloud fraction used in most SCMs (Table 2). *Xu and Randall* [1996] proposed a fractional cloud parameterization, in which cloud fraction is directly related to condensate mixing ratio. The decoupling between these two quantities cannot happen when this parameterization is used because RH is only used to determine the slope of the variation between cloud fraction and cloud condensate. This may be a possible direction for cloud parameterizations in SCMs/GCMs. The small amount of cloud condensate above 500 hPa in all SCM simulations results from a dissipation process that is explicitly formulated in cloud parameterizations. A positive tendency in the saturation mixing ratio (*Sundqvist* [1978]; Table 2) reduces the LWC while the cloud fraction is assumed to be unchanged. The positive tendency is due to the imposed large-scale subsidence in the upper troposphere during parts of the SF period (Figure 7a), but this subsidence is not strong

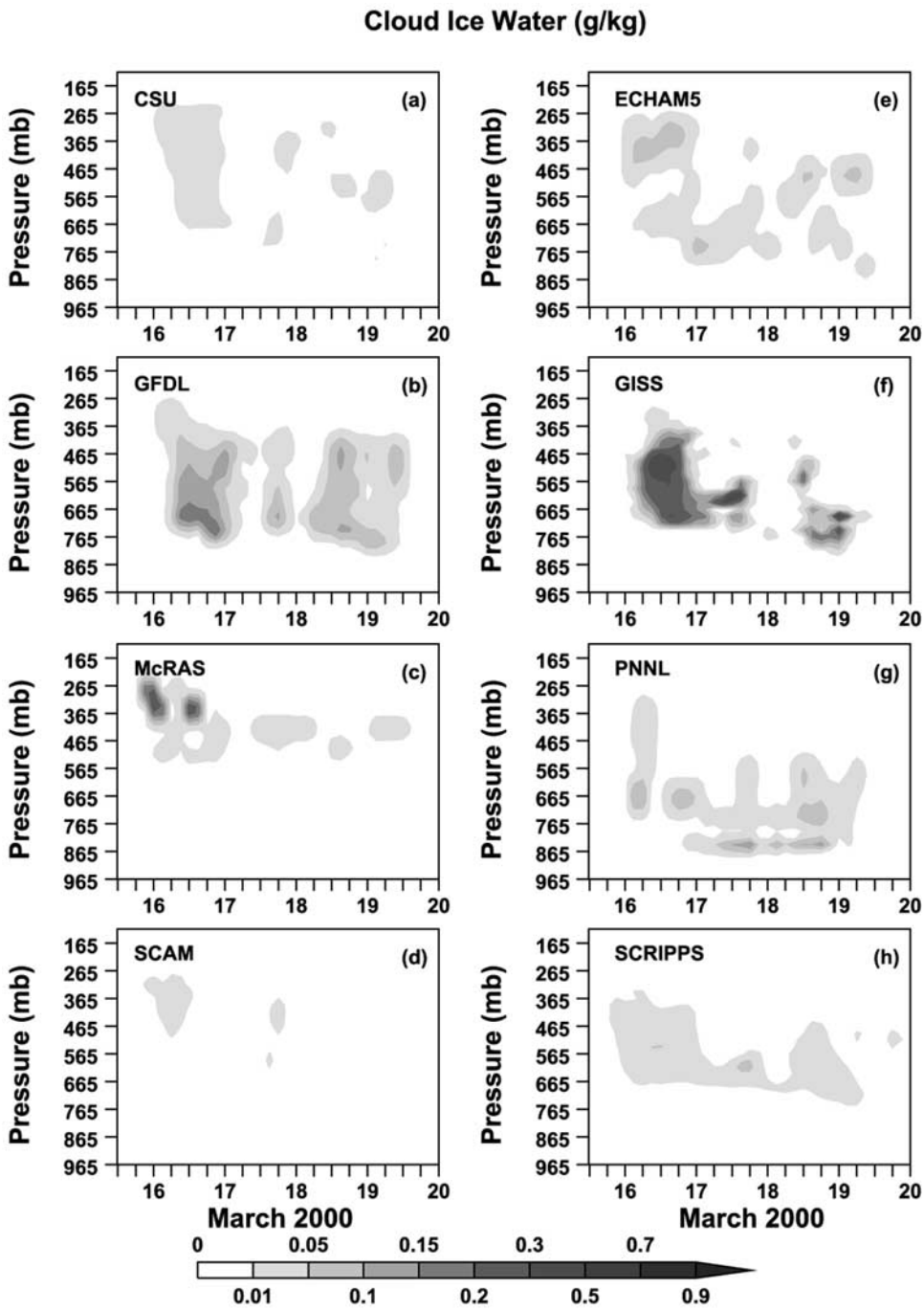

Figure 18. Time-pressure cross section of the cloud ice water content simulated by SCMs: (a) CSU, (b) GFDL, (c) McRAS, (d) SCAM, (e) ECHAM5, (f) GISS, (g) PNNL, and (h) Scripps.

enough to cause significant reduction of the RHs in the SCMs.

[54] Third, the errors in the simulated thermodynamic soundings at the beginning of this period are too large to overcome so that clouds have to be produced in the SCMs because of the initial cold biases of up to 7 K (Figure 19d), which increase the RH there. The averaged cold biases are ~2 K higher in most SCMs for the SF period, compared to the initial cold biases (Figure 10d). The high RHs exceed the threshold values, which produce nonzero cloud fraction in spite of the lack of cloud ice in most SCMs except for the ECHAM5 SCM, which directly couples the cloud fraction with condensate using a prognostic PDF approach [*Tompkins*, 2002].

[55] Why does the large overestimate in cloud fraction occur between 765 hPa and 500 hPa in all SCMs except for the CSU, McRAS and SCAM SCMs while three of the CRMs simulate the right amount of clouds there? One of the possible explanations is the uncertainties in fractional cloud parameterization: the small threshold RHs, the linear relations between cloud fraction and RH, and the overestimate of LWC and/or IWC. The McRAS and SCAM SCMs do not

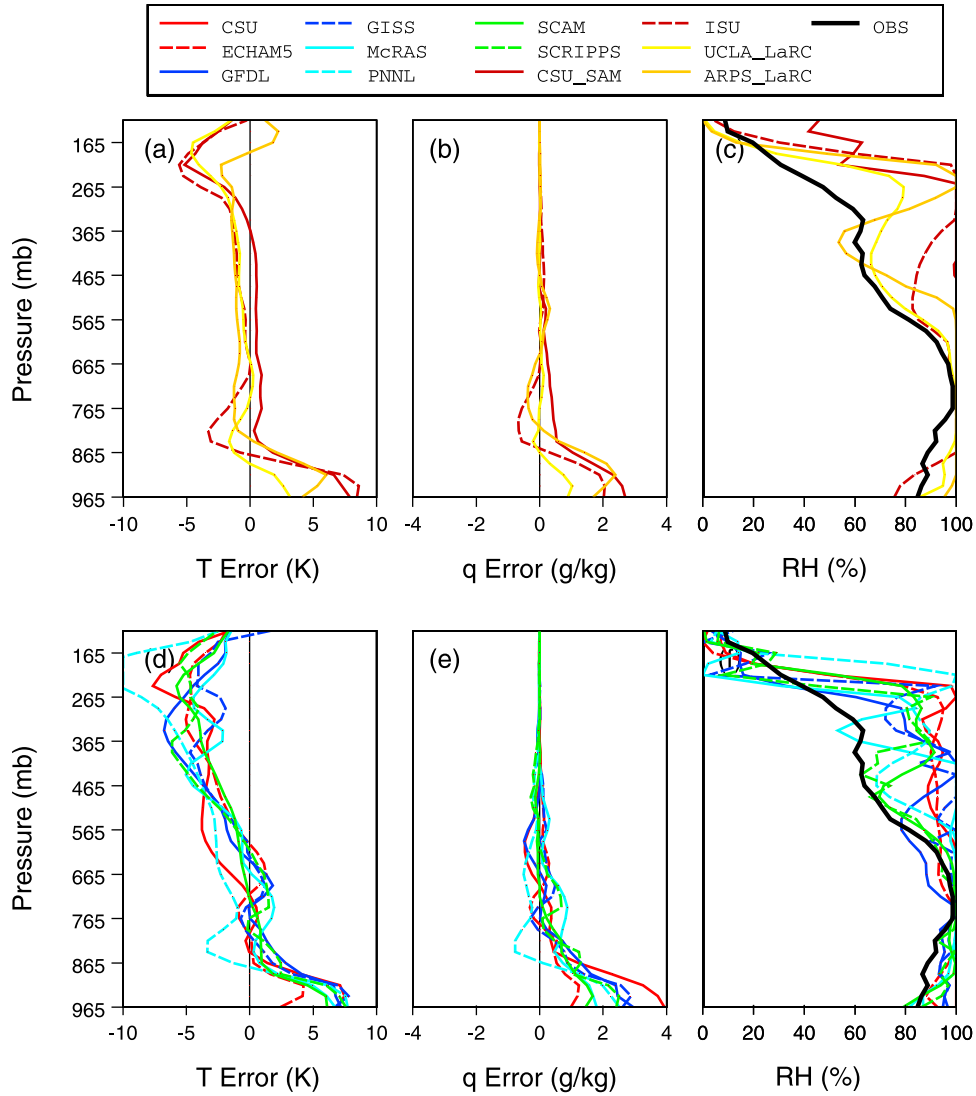

Figure 19. Vertical profiles of temperature and water vapor mixing ratio deviations from the observed and the simulated and observed relative humidity at 0000 UT 17 March from (a–c) CRMs and (d–f) SCMs.

overestimate the cloud fraction in this layer by much because they use a cloud fraction-dependent RH threshold. This formulation raises the threshold RH when the cloud fraction increases. They also use a quadratic relationship between cloud fraction and RH. With the prognostic PDF approach, the ECHAM5 SCM also overestimates the cloud fraction, which is related to the overestimate of LWC in this layer (Figure 17e). The *Tiedtke* [1993] scheme also tends to overestimate the cloud fraction in the Scripps and GFDL SCMs. The latter SCM only uses the Tiedtke scheme for predicting cloud fraction but the LWC/IWC is predicted with a separate scheme. The LWC simulated by the GFDL SCM is overestimated but that of the Scripps SCM is underestimated. The initially overestimated cloud fraction in the GFDL SCM cannot decrease due to the lack of dissipation mechanism in the *Tiedtke* [1993] scheme.

[56] The second explanation is that the overestimated cloud fraction is enhanced by cloud-radiation interactions in some of the SCMs. The radiative cooling rates averaged over the 27-hour period are larger in those SCMs with large overestimates of cloud fractions between 765 hPa and 500 hPa (Figure 20). The temperature biases in most SCMs are slightly larger than those in the CRMs and those before the SF period begins (Figures 10 and 19). The temperature and RH biases at 0000 UT 17 March are much smaller than those of the averaged biases over the SF period. This is true for both SCMs and CRMs. The relationship between the temperature biases and radiative cooling rates is, however, complicated by the effect of latent heat release.

4.4. Summary

[57] The four specific questions formulated at the beginning of this section can be answered as follows. Both CRMs and SCMs can generally simulate the observed vertical profiles of cloud fraction and cloud microphysical properties for this case study. The magnitudes of cloud fractions are, however, underestimated slightly more strongly in the CRMs than in some of the SCMs for both deep and shallow frontal cloud systems. Most of the SCMs also produce significant amounts of middle- and high-level

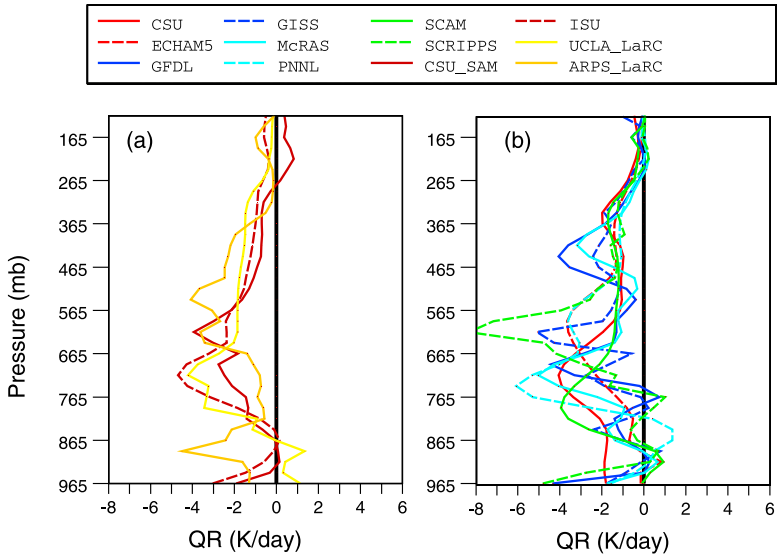

Figure 20. Vertical profiles of radiative heating rates averaged over the SF period for (a) CRMs and (b) SCMs.

clouds while all CRMs do not when only shallow frontal clouds are observed. The general characteristics of the observed shallow frontal clouds are well simulated in two of the CRMs. The magnitudes of cloud microphysical properties, LWC and IWC, agree basically with the observations for most of the participating models. The degree of agreement in the temporal evolutions and vertical extents of LWC and IWC between simulations and observations is rather different from one model to another.

[58] Physical causes for the inadequate simulations of shallow clouds in SCMs may include (1) the decoupling of the cloud fraction with condensate mixing ratio in most of the SCMs, except for the CSU and ECHAM5 SCM, (2) the inadequate formulation of cloud microphysical processes such as the autoconversion process, (3) the deficiencies in fractional cloud parameterizations, (4) the lack of advective forcings organized at the mesoscale level and the lack of horizontal advection of hydrometeors, and (5) the errors in the simulated thermodynamic soundings prior to the SF period. The discrepancies between simulations and observations may also be amplified by cloud-radiation interactions and they are also related to the unresolved upper tropospheric dynamical forcings. In CRMs, possible reasons for the inadequate simulations are the dynamical frameworks and the inadequate formulations of some cloud microphysical processes, in addition to the uncertainties in the imposed forcings.

[59] The main reasons for the intermodel differences may be related to the 2-D configuration of the CRMs and their different dynamical frameworks and treatments of cloud microphysical processes, the different formulations of cloud microphysical processes in SCMs including the transition from liquid to ice phases and the detailed treatments of some key processes (see section 2), the different formulations of fractional cloud parameterizations in SCMs including the decoupling of condensate with cloud fraction, and the different treatments of shallow cumulus convection in the SCMs. The latter has not been discussed much in this study. It seems to be a good candidate for explaining the intermodel differences in simulating the shallow frontal clouds because of the diversified representations of shallow cumulus processes used in the SCMs.

[60] Finally, the CRMs do not necessarily perform much better than the SCMs for the shallow frontal cloud systems although two of the CRMs with anelastic dynamical frameworks simulate them rather well. This is a surprising conclusion because CRMs performed much better than SCMs for simulations of summertime cumulus convection [*Xie et al.*, 2002; *Xu et al.*, 2002].

5. Conclusions and Discussion

[61] This modeling study has extensively compared the performance of eight SCMs and four CRMs in simulating shallow frontal cloud systems observed during a period of the March 2000 ARM IOP. Except for the passage of a cold front at the beginning of this period, the frontal cloud systems were under the influence of an upper tropospheric ridge and driven by a persistent frontogenesis over the Southern Great Plains and moisture transport from the northwestern part of the Gulf of Mexico. Frontal cloud systems propagated through the ARM CART domain during most of the four and a half day period. Thus horizontal advection rather than local generation of shallow frontal clouds was the main characteristic of the cloud systems modeled by several CRMs and SCMs in this study. This study has presented quantitative comparisons among model simulations, with a focus on a 27 hour period when only shallow frontal clouds were observed.

[62] All CRMs and SCMs simulate clouds in the observed shallow cloud layer. Most SCMs also produce clouds in the middle and upper troposphere while none of the CRMs produce any clouds there. There are several possible explanations for this. One of them is that the imposed large-scale dynamical forcing is not strong enough to suppress the residual middle-level clouds from the early deep frontal cloud systems in most SCMs. The second explanation is that there is a decoupling between cloud

condensate and cloud fraction in all SCM parameterizations except for the CSU and ECHAM5 SCM. Clouds are produced whenever RHs, which are overestimated in both the CRMs and SCMs, reach the thresholds despite the cloud water/ice content is almost nonexistent. The third explanation is that the simulated errors in the thermodynamic soundings prior to the SF period are too large to overcome so that clouds are produced in the SCMs.

[63] All CRMs and most SCMs underestimate shallow clouds in the lowest 125 hPa near the surface, but most SCMs also overestimate shallow clouds above. Intermodel differences may be related to the dynamical framework and limitations in the 2-D configuration of the CRMs, but are related mainly to the differences in the cloud microphysical parameterizations among the SCMs. Three-dimensional CRMs may alleviate the problems in the 2-D configuration of CRMs so that mesoscale frontal circulations can be better simulated. The underestimates of LWCs by four of the SCMs are likely related to the Sundqvist-type formulation of the autoconversion process or the small threshold for autoconversion although other microphysical processes may not be ruled out, based upon the comparison between the observed and simulated LWCs. Two other SCMs simulate the cloud fraction much better in the upper part of the shallow cloud layer because they use a cloud fraction-dependent RH threshold and a quadratic relationship between cloud fraction and RH, instead of the linear relationship adopted in some SCMs. The *Tiedtke* [1993] prognostic cloud parameterization also overestimates the cloud fraction in two of the SCMs, due to the lack of cloud dissipative mechanisms. It has been argued in this study that cloud condensate and cloud fraction should be directly linked in the future if diagnostic fractional cloud parameterizations continue to be used in climate models. Such an approach has been advocated in the work of *Xu and Randall* [1996]. Ideally, cloud fraction should be prognostically determined provided that its source and sink terms are well understood and properly formulated.

[64] For the simulations of the entire period with both shallow and deep frontal clouds, a few distinct characteristics of the simulations have been identified. First, the CRM results show a vertical phase tilting in the cloud fractions, especially above the shallow frontal cloud layer, while the SCM results show a vertical phase tilting in the LWC. The single-point measurements of cloud property profiles do not have any vertical phase tilting. Second, the peak magnitudes of the simulated cloud properties are underestimated in most models and the life cycles of the deep frontal cloud systems are longer than the observed ones. Both results suggest the importance of having the spatial structures of the dynamical forcings and the horizontal advection of hydrometeors, which are currently not available, to drive model simulations and to adequately evaluate the performance of the models. Additionally, cloud-radiation interactions may also amplify the discrepancies between the SCM simulations and observations.

[65] Finally, intermodel differences in the SCM-simulated cloud properties and their profiles are still as large as those of summertime continental convection [*Xie et al.*, 2002; *Xu et al.*, 2002], but the intermodel differences in the thermodynamic profiles are comparable between the CRMs and SCMs for this case study. Overall, not all CRMs perform much better than the SCMs do. This result has some serious implications to the super parameterization approach, in which a 2-D CRM is embedded in a grid box of a climate model [*Grabowski*, 2001; *Khairoutdinov and Randall*, 2001], as far as frontal cloud systems are concerned. Nevertheless, the availability of these cloud microphysical property profile measurements will be very valuable for individual modelers to further improve their cloud parameterizations in the SCMs and cloud microphysics parameterizations in the CRMs.

[66] **Acknowledgments.** This study has been primarily supported by the Department of Energy's Atmospheric Radiation Measurement program, under interagency agreement DE-AI02-02ER63318 (Xu), grant DE-FG-02-98ER62570 (M. Zhang and Lin), contract DE-AC06-76RL01830 (Ghan), interagency agreement DE-AI02-03ER63562 (Klein), contract W-7405-Eng-48 (Xie and Yio), grant DE-FG02-02ER63483 (Wu), grant DE-FG03-91ER61198 (Branson, Khairoutdinov and Randall), interagency agreement DE-AI02-94ER61768 (Del Genio and Wolf), and grant DE-FG03-97-ER62338 (Iacobellis and Somerville). Work at Dalhousie University, Canada (Lohmann and J. Zhang), was supported by the MOC2 project jointly funded by NSEC, CFCAS, and MSC. Work at Goddard Space Flight Center (Sud and Walker) was supported by the GMAP program NASA HQ funding. Work at Langley Research center (Eitzen and Xu) was also supported by the NASA EOS interdisciplinary study program. Work at SUNY Stony Brook was also supported by NSF under grant ATM9701950. Work at Scripps (Iacobellis and Somerville) was also supported by NOAA under grant NA77RJO453 and by NSF under grant ATM-9613764. The satellite data used in this study are available from the Pat Minnis group at NASA Langley Research Center (http://angler.larc.nasa.gov/armsgp/).

References

Ackerman, T. P., and G. M. Stokes (2003), The Atmospheric Radiation Measurement Program, *Phys. Today*, *56*, 38–44.

Bechtold, P., et al. (2000), A GCSS model intercomparison for a tropical squall line observed during TOGA-COARE. Part II: Intercomparison of single-column models with a cloud-resolving model, *Q. J. R. Meteorol. Soc.*, *126*, 865–888.

Beheng, K. D. (1994), A parameterization of warn cloud microphysical conversion processes, *Atmos. Res.*, *33*, 193–206.

Bénard, P., J.-P. Redeslsperger, and J.-P. Lafore (1992), Nonhydrostatic simulation of frontogenesis in a moist atmosphere. Part I: General description and narrow rainbands, *J. Atmos. Sci.*, *49*, 2200–2217.

Berry, E. X. (1968), Modification of the warm rain process, in *Proceedings of 1st National Conference on Weather Modification*, pp. 81–85, Am. Meteorol. Soc., Boston, Mass.

Bony, S., and K. A. Emanuel (2001), A parameterization of the cloudiness associated with cumulus convection: Evaluation using TOGA COARE data, *J. Atmos. Sci.*, *58*, 3158–3183.

Clark, T. L., W. D. Hall, and R. M. Banta (1994), Two- and three-dimensional simulations of the 9 January 1989 severe Boulder windstorm: Comparison with observations, *J. Atmos. Sci.*, *51*, 2317–2343.

Clothiaux, E. E., K. P. Moran, B. E. Martner, T. P. Ackerman, G. G. Mace, T. Uttal, J. H. Mather, K. B. Widener, M. A. Miller, and D. J. Rodriguez (1999), The Atmospheric Radiation Measurement program cloud radars: Operational modes, *J. Atmos. Oceanic Technol.*, *16*, 819–827.

Cotton, W. R., G. J. Tripoli, R. M. Rauber, and E. A. Mulvihill (1986), Numerical simulation of the effects of varying ice crystal nucleation rates and aggregation processes on orographic snowfall, *J. Clim. Appl. Meteorol.*, *25*, 1658–1680.

Del Genio, A. D., M.-S. Yao, W. Kovari, and K. K.-W. Lo (1996), A prognostic cloud water parameterization for global climate models, *J. Clim.*, *9*, 270–304.

Del Genio, A. D., W. Kovari, M.-S. Yao, and J. Jonas (2005), Cumulus microphysics and climate sensitivity, *J. Clim.*, in press.

Dong, X., and G. G. Mace (2003), Profiles of low-level stratus cloud microphysics deduced from ground-based measurements, *J. Atmos. Oceanic Technol.*, *20*, 42–53.

Fowler, L. D., D. A. Randall, and S. A. Rutledge (1996), Liquid and ice cloud microphysics in the CSU general circulation model. Part I: Model description and simulated microphysical processes, *J. Clim.*, *9*, 489–529.

Ghan, S. J., L. R. Leung, and Q. Hu (1997), Application of cloud microphysics to NCAR CCM2, *J. Geophys. Res.*, *102*, 16,507–16,527.

Ghan, S. J., et al. (2000), An intercomparison of single column model simulations of summertime midlatitude continental convection, *J. Geophys. Res.*, *105*, 2091–2124.

Grabowski, W. W. (2001), Coupling cloud processes with the large-scale dynamics using the cloud-resolving convection parameterization (CRCP), *J. Atmos. Sci.*, *58*, 978–997.

Iacobellis, S. F., G. M. McFarquhar, D. L. Mitchell, and R. J. C. Somerville (2003), The sensitivity of radiative fluxes to parameterized cloud microphysics, *J. Clim.*, *16*, 2979–2996.

Kessler, E. (1969), *On the Distribution and Continuity of Water Substance in Atmospheric Circulation*, *Meteorol. Monogr. Ser.*, vol. 32, 84 pp., Am. Meteorol. Soc., Boston, Mass.

Khairoutdinov, M. F., and Y. Kogan (2000), A new cloud physics parameterization in a large-eddy simulation model of marine stratocumulus, *Mon. Weather Rev.*, *118*, 229–243.

Khairoutdinov, M. F., and D. A. Randall (2001), A cloud-resolving model as a cloud parameterization in the NCAR Community Climate System Model: Preliminary results, *Geophys. Res. Lett.*, *28*, 3617–3620.

Khairoutdinov, M., and D. A. Randall (2003), Cloud-resolving modeling of the ARM summer 1997 IOP: Model formulation, results, uncertainties and sensitivities, *J. Atmos. Sci.*, *60*, 607–625.

Klein, S. A., and C. Jakob (1999), Validation and sensitivities of frontal clouds simulated by the ECMWF model, *Mon. Weather Rev.*, *127*, 2514–2531.

Koenig, L. R., and F. W. Murray (1976), Ice-bearing cumulus cloud evolution: Numerical simulation and general comparison against observations, *J. Appl. Meteorol.*, *15*, 747–762.

Krueger, S. K., Q. Fu, K.-N. Liou, and H.-N. Chin (1995), Improvements of an ice-phase microphysics parameterization for use in numerical simulations of tropical convection, *J. Appl. Meteorol.*, *34*, 281–287.

Lin, Y.-L., R. D. Farley, and H. D. Orville (1983), Bulk parameterization of the snow field in a cloud model, *J. Clim. Appl. Meteorol.*, *22*, 1065–1092.

Lohmann, U., and E. Roecker (1996), Design and performance of a new cloud microphysics scheme developed for the ECHAM general circulation model, *Clim. Dyn.*, *12*, 557–572.

Lohmann, U., J. Feichter, C. C. Chuang, and J. E. Penner (1999), Predicting the number of cloud droplets in the ECHAM GCM, *J. Geophys. Res.*, *104*, 9169–9198.

Manton, M. J., and W. R. Cotton (1977), Formulation of approximate equations for modeling moist deep convection on the mesoscale, *Atmos. Sci. Pap. 266*, Dept. of Atmos. Sci., Colo. State Univ., Fort Collins, Colo.

Miller, M. A., K. L. Johnson, M. P. Jensen, G. G. Mace, X. Dong, and A. M. Vogelmann (2004), A Continuous Baseline Microphysical Retrieval (MICROBASE): Status of SGP version 1.2 and prototype TWP version, paper presented at 14th ARM Science Team Meeting, Atmos. Radiat. Measure. Prog., Dept. of Energy, Albuquerque, N. M.

Moncrieff, M. W., S. K. Krueger, D. Gregory, J.-L. Redelsperger, and W.-K. Tao (1997), GEWEX Cloud System Study (GCSS) Working Group 4: Precipitating convective cloud systems, *Bull. Am. Meteorol. Soc.*, *78*, 831–845.

Moran, K. P., B. E. Martner, M. J. Post, R. A. Kropfli, D. C. Welsh, and K. B. Widener (1998), An unattended cloud-profiling radar for use in climate research, *Bull. Am. Meteorol. Soc.*, *79*, 443–455.

Ovtchinnikov, M., and S. J. Ghan (2005), Parallel simulations of aerosol influence on clouds using cloud-resolving and single-column models, *J. Geophys. Res.*, *110*, D15S10, doi:10.1029/2004JD005088.

Petch, J. C., and J. Dudhia (1998), The importance of the horizontal advection of hydrometeors in a single-column model, *J. Clim.*, *11*, 2437–2452.

Randall, D. A., K.-M. Xu, R. C. J. Somerville, and S. Iacobellis (1996), Single-column models and cloud ensemble models as links between observations and climate models, *J. Clim.*, *9*, 1683–1697.

Rasch, P. J., and J. E. Kristjánsson (1998), A comparison of the CCM3 model climate using diagnosed and predicted condensate parameterizations, *J. Clim.*, *11*, 1587–1614.

Redelsperger, J.-L., et al. (2000), A GCSS model intercomparison for a tropical squall line observed during TOGA-COARE. I: Cloud-resolving models, *Q. J. R. Meteorol. Soc.*, *115*, 823–864.

Rotstayn, L. D. (1997), A physical based scheme for the treatment of stratiform clouds and precipitation in large-scale models. I: Description and evaluation of the microphysical processes, *Q. J. R. Meteorol. Soc.*, *123*, 1227–1282.

Rotstayn, L. D., B. F. Ryan, and J. J. Katzfey (2000), A scheme for calculation of the liquid fraction in mixed-phase stratiform clouds in large-scale models, *Mon. Weather Rev.*, *128*, 1070–1088.

Rutledge, S. A., and P. V. Hobbs (1984), The mesoscale and microscale structure and organization of clouds and precipitation in midlatitude cyclones. XII: A diagnostic modeling study of precipitation development in narrow cold-frontal rainbands, *J. Atmos. Sci.*, *41*, 2949–2972.

Ryan, B. F., et al. (2000), Simulations of a cold front by cloud-resolving, limited-area, and large-scale models, and a model evaluation using in situ and satellite observations, *Mon. Weather Rev.*, *128*, 3128–3135.

Simpson, J., and V. Wiggert (1969), Models of precipitating cumulus towers, *Mon. Weather Rev.*, *97*, 471–489.

Smith, R. N. B. (1990), A scheme for predicting layer clouds and their water content in a GCM, *Q. J. R. Meteorol. Soc.*, *113*, 435–460.

Stokes, G. M., and S. E. Schwartz (1994), The Atmospheric Radiation Measurement (ARM) program: Programmatic background and design of the cloud and radiation test bed, *Bull. Am. Meteorol. Soc.*, *75*, 1202–1221.

Sud, Y. C., and G. K. Walker (1999), Microphysics of clouds with the relaxed Arakawa-Schubert scheme (McRAS). Part I, Design and evaluation with GATE Phase III data, *J. Atmos. Sci.*, *56*, 3196–3220.

Sundqvist, H. (1978), A parameterization scheme for non-convective condensation including prediction of cloud water content, *Q. J. R. Meteorol. Soc.*, *104*, 677–690.

Sundqvist, H., E. Berge, and J. E. Kristjánsson (1989), Condensation and cloud parameterization studies with a mesoscale numerical weather prediction model, *Mon. Weather Rev.*, *117*, 1641–1657.

Tiedtke, M. (1993), Representation of clouds in large-scale models, *Mon. Weather Rev.*, *121*, 3040–3061.

Tompkins, A. M. (2002), A prognostic parameterization for the subgrid-scale variability of water vapor and clouds in large-scale model and its use to diagnose cloud cover, *J. Atmos. Sci.*, *59*, 1917–1942.

Xie, S., et al. (2002), Intercomparison and evaluation of GCM cumulus parameterizations under summertime midlatitude continental conditions, *Q. J. R. Meteorol. Soc.*, *128*, 1095–1135.

Xie, S., et al. (2005), Simulations of midlatitude frontal clouds by single-column and cloud-resolving models during the Atmospheric Radiation Measurement March 2000 cloud intensive operational period, *J. Geophys. Res.*, *110*, D15S03, doi:10.1029/2004JD005119.

Xu, K.-M., and D. A. Randall (1996), A semiempirical cloudiness parameterization for use in climate models, *J. Atmos. Sci.*, *58*, 3084–3102.

Xu, K.-M., et al. (2002), An intercomparison of cloud-resolving models with the Atmospheric Radiation Measurement summer 1997 IOP data, *Q. J. R. Meteorol. Soc.*, *128*, 593–624.

Xue, M., K. K. Droegemeier, V. Wong, A. Shapiro, K. Brester, F. Carr, D. Weber, Y. Liu, and D.-H. Wang (2001), The Advanced Regional Prediction System (ARPS)—A multi-scale nonhydrostatic atmospheric simulation and prediction tool. Part II: Model physics and application, *Meteorol. Atmos. Phys.*, *76*, 143–165.

Zhang, M., and J. L. Lin (1997), Constrained variational analysis of sounding data based on column-integrated budgets of mass, heat, moisture, and momentum: Approach and application to ARM measurements, *J. Atmos. Sci.*, *54*, 1503–1524.

Zhang, M., J. L. Lin, R. T. Cederwall, J. J. Yio, and S. C. Xie (2001), Objective analysis of ARM IOP data: Method, feature and sensitivity, *Mon. Weather Rev.*, *129*, 295–311.

Zhang, M., W. Lin, C. S. Bretherton, J. J. Hack, and P. J. Rasch (2003), A modified formulation of fractional stratiform condensation rate in the NCAR Community Atmospheric Model (CAM2), *J. Geophys. Res.*, *108*(D1), 4035, doi:10.1029/2002JD002523.

M. Branson, M. Khairoutdinov, and D. A. Randall, Department of Atmospheric Science, 200 W. Lake Street, Colorado State University, Fort Collins, CO 80523-1371, USA. (mark@atmos.colostate.edu; marat@atmos.colostate.edu; randall@atmos.colostate.edu)

A. D. Del Genio and A. Wolf, NASA Goddard Institute for Space Studies, 2880 Broadway, New York, NY 10025, USA. (adelgenio@giss.nasa.gov; awolf@thelma.giss.nasa.gov)

Z. A. Eitzen and K.-M. Xu, Climate Science Branch, NASA Langley Research Center, Mail Stop 420, Hampton, VA 23681, USA. (z.a.eitzen@larc.nasa.gov; kuan-man.xu@nasa.gov)

S. J. Ghan, Atmospheric Sciences Division, Pacific Northwest National Laboratory, Mail Stop K9-24, PO Box 999, Richland, WA 99352, USA. (steve.ghan@pnl.gov)

S. F. Iacobellis and R. C. J. Somerville, Scripps Institution of Oceanography, University of California, San Diego, La Jolla, CA 92093-0224, USA. (siacobellis@ucsd.edu; rsomerville@ucsd.edu)

S. A. Klein, S. Xie, and J. J. Yio, Atmospheric Science Division (L-103), Lawrence Livermore National Laboratory, Livermore, CA 94551, USA. (klein21@llnl.gov; xie2@llnl.gov; yio1@llnl.gov)

W. Lin and M. Zhang, Institute for Terrestrial and Planetary Atmospheres, Marine Sciences Research Center, Stony Brook University, Stony Brook, NY 11794-5000, USA. (wlin@atmsci.msrc.sunysb.edu; mzhang@notes.cc.sunysb.edu)

Ü. Löhmann, Institute for Atmospheric and Climate Science, Eidgenossische Technische Hochschule, Zurich, Switzerland. (ulrike.lohmann@env.ethz.ch)

Y. C. Sud and G. K. Walker, Climate and Radiation Branch, Laboratory for Atmospheres, NASA GSFC, Greenbelt, MD 20771, USA. (sud@climate.gsfc.nasa.gov; walker@climate.gsfc.nasa.gov)

X. Wu, Department of Geological and Atmospheric Sciences, Iowa State University, 3010 Agronomy Hall, Ames, IA 50011-1010, USA. (wuxq@iastate.edu)

J. Zhang, Department of Physics and Atmospheric Science, Dalhousie University, Halifax, Nova Scotia, Canada B3H 3C3. (zhang@mathstat.dal.ca)